MOZ directs the distal-less homeobox gene expression program during craniofacial development

Hannah K. Vanyai[1,2], Alexandra Garnham[1], Rose E. May[1], Helen M. McRae[1,2], Caitlin Collin[1], Stephen Wilcox[1], Gordon K. Smyth[1,3], Tim Thomas[1,2,*,‡] and Anne K. Voss[1,2,*,‡]

ABSTRACT

Oral clefts are common birth defects. Individuals with oral clefts who have identical genetic mutations regularly present with variable penetrance and severity. Epigenetic or chromatin-mediated mechanisms are commonly invoked to explain variable penetrance. However, specific examples of these are rare. Two functional copies of the *MOZ* (*KAT6A*, *MYST3*) gene, encoding a MYST family lysine acetyltransferase chromatin regulator, are essential for human craniofacial development, but the molecular role of MOZ in this context is unclear. Using genetic interaction and genomic studies, we have investigated the effects of loss of MOZ on the gene expression program during mouse development. Among the more than 500 genes differentially expressed after loss of MOZ, 19 genes had previously been associated with cleft palates. These included four distal-less homeobox (DLX) transcription factor-encoding genes, *Dlx1*, *Dlx2*, *Dlx3* and *Dlx5* and DLX target genes (including *Barx1*, *Gbx2*, *Osr2* and *Sim2*). MOZ occupied the *Dlx5* locus and was required for normal levels of histone H3 lysine 9 acetylation. MOZ affected Dlx gene expression cell-autonomously within neural crest cells. Our study identifies a specific program by which the chromatin modifier MOZ regulates craniofacial development.

KEY WORDS: Craniofacial development, Cleft palate, MOZ, KAT6A, DLX, Histone acetylation, Chromatin

INTRODUCTION

Craniofacial development is a complex process involving the outgrowth of five distinct prominences: the frontonasal prominence, the paired maxillary processes and the paired mandibular processes. These processes need to grow in a concerted manner at a specific rate and then fuse in the midline to form normal facial structures (reviewed by Dixon et al., 2011; Lan et al., 2015). A reduction in growth, an increase or decrease in cell death (e.g. Grabow et al., 2018; Ke et al., 2018) or a failure of midline fusion can result in craniofacial anomalies, including small upper and lower jaws, misalignment of teeth, cleft lip and/or palate.

The palate divides the nasal and oral cavities, and so separates the airway from the mouth. Its development commences with the formation of the primary palate from the medial nasal prominences (reviewed by Bush and Jiang, 2012; Gritli-Linde, 2008). The secondary palate arises from the maxillary component of the first pharyngeal arch, develops as horizontal outgrowths on the oral side of the maxillary processes [in mice at embryonic day (E) 11.0] and continues with vertical growth down alongside the tongue (at E13.5). The palatal shelves elevate (at E14.5) until they lie horizontally above the tongue and then grow horizontally and fuse in the midline (Gritli-Linde, 2007; Walker and Fraser, 1956; Yu and Ornitz, 2011).

Failure of secondary palate development leads to cleft palate. Oral clefts, including cleft lip and cleft of the secondary palate, occur at a rate of 1 in 500-2500 live births, causing problems with feeding, speaking, hearing and social integration (Dixon et al., 2011). Phenotypic concordance of oral cleft in monozygotic twins has been reported as 31% (Grosen et al., 2011), indicative of genetic as well as non-genetic contributions to the cause of the disorder. Chromatin modifiers have been proposed to mediate environmental effects on gene expression. A small number of genes encoding chromatin-modifying or chromatin-associated proteins has been associated with cleft palate, suggesting that they may be involved in epigenetic or chromatin-mediated mechanisms that affect palate development. The proteins include MEN1 (Engleka et al., 2007), which is associated with the MLL/SET1 H3K4 methyltransferase complex, the H3K9me1/2 methyltransferase PHF8 (Fortschegger et al., 2010; Laumonnier et al., 2005; Loenarz et al., 2010), the chromodomain helicase DNA binding protein CHD7 (Sperry et al., 2014), the H3K4me and H3K9me demethylase KDM1A (Tunovic et al., 2014), the H3K27me demethylase KDM6A (Lindgren et al., 2013) and the lysine acetyltransferase KAT6B (Campeau et al., 2012; Clayton-Smith et al., 2011). Although their biochemical function is known, their molecular effects on palate development remain unclear except in the case of MEN1 (Engleka et al., 2007).

Heterozygous mutations of the chromatin modifier gene *KAT6A* (also known as *MOZ* and *MYST3*) have been found to cause a congenital disorder characterised by craniofacial anomalies (including cleft palate at low penetrance), heart defects and developmental delay (Arboleda et al., 2015; Millan et al., 2016; Tham et al., 2015). *KAT6A* encodes the histone lysine acetyltransferase monocytic leukaemia zinc-finger protein (MOZ) and was originally identified as the target of recurrent chromosomal translocations causing an aggressive form of acute myeloid leukaemia (Borrow et al., 1996). Null mutation of the *Moz* (*Kat6a/Myst3*) gene in mice causes haematological anomalies, characterised by a complete absence of definitive haematopoietic stem cells (Katsumoto et al., 2006; Sheikh et al., 2016; Thomas et al., 2006), and specific defects in B-cell (Good-Jacobson et al., 2014; Sheikh et al., 2015b) and T-cell development (Newman et al., 2016). In addition, loss of MOZ causes developmental defects, including body segment identity, craniofacial and heart defects. Mice lacking MOZ have micrognathia, a complete secondary palate cleft (100% penetrance), an extensive anterior

[1]Walter and Eliza Hall Institute of Medical Research, Melbourne, Parkville, VIC 3052, Australia. [2]Department of Medical Biology, University of Melbourne, Parkville, VIC 3052, Australia. [3]Department School of Mathematics and Statistics, University of Melbourne, Parkville, VIC 3052, Australia.
*These authors contributed equally this work and share senior authorship

‡Authors for correspondence (avoss@wehi.edu.au; tthomas@wehi.edu.au)

G.K.S., 0000-0001-9221-2892; A.K.V., 0000-0002-3853-9381

homeotic transformation affecting 19 body segments, as well as aortic arch and cardiac ventricular septum defects (Vanyai et al., 2015; Voss et al., 2009, 2012). Similarly, MOZ is required to determine pharyngeal segmental identity in zebrafish (Crump et al., 2006; Miller et al., 2004).

MOZ target genes relevant for the correct specification of body segment identity and for normal heart development have been identified. MOZ is required for normal levels of histone 3 lysine 9 acetylation (H3K9ac) and for transcription of Hox genes, which are crucial for correct specification of segment identity. Induction of Hox gene expression with retinoic acid rescues the segment identity defects in $Moz^{-/-}$ mice, but not the craniofacial defects (Voss et al., 2009). Similarly, for cardiac septum development, MOZ is essential for normal levels of H3K9ac and transcription at the $Tbx1$ gene locus; transgenic overexpression of $Tbx1$ rescues cardiac septum defects in $Moz^{-/-}$ mice, but not the craniofacial defects (Voss et al., 2012). Thus, while MOZ target genes required for body segment identity specification and heart development are known, the effects of MOZ on the transcriptional program in the complex process of craniofacial and palate development are unknown. Unlike many other aspects of facial dysmorphogenesis, oral clefts (cleft lip/cleft palate) are clearly defined birth defects, and so we concentrated on this particular aspect of the Moz mutant craniofacial defects. Here, we report that MOZ is an activator of gene expression, including the $Dlx5$ gene, and of the DLX transcription factor-induced gene expression program during craniofacial development.

RESULTS

Moz mRNA is expressed widely in most or all cells at all stages of mouse embryonic development examined (E7.5, E8.5, E9.5, E10.5 and E13.5), including in the maxillary component of the first pharyngeal arch, which gives rise to the secondary palate (Sheikh et al., 2015a; Thomas et al., 2006; Voss et al., 2009). We have previously reported craniofacial defects in MOZ-deficient mouse

foetuses, including micrognathia and a complete cleft of the secondary palate (Voss et al., 2012).

Moz deficiency results in small palatal shelves

Frontal serial sections of the heads prior to (E13.5), during (E14.5) and immediately after (E15.5) palatal shelf elevation revealed that the palatal shelves of $Moz^{+/+}$ littermate control and Moz exon 16 truncated $Moz^{\Delta/\Delta}$ mutants (no protein detectable, therefore null) occupied a similar position at E13.5 (Fig. 1A,B), but that the $Moz^{\Delta/\Delta}$ shelves had slightly reduced cross-sections of the intermediate region (105,985±2266 μm² versus 115,543±1569 μm², P=0.026, n=3 animals per genotype). At E14.5, the palatal shelves of wild-type foetuses had completed elevation and fused along the midline (Fig. 1C). In contrast, the palatal shelves of the $Moz^{\Delta/\Delta}$ mutants were smaller and had not elevated to a horizontal orientation above the tongue (Fig. 1D), indicating a defect in growth and elevation of the shelves at this stage. At E15.5, the palatal shelves of $Moz^{\Delta/\Delta}$ foetuses had elevated, but remained apart, resulting in a wide cleft (compare Fig. 1F with E,G).

Cell death within the palatal shelves was not affected by the absence of MOZ (Fig. 1H). Assessment of BrdU incorporation at rostral, intermediate and caudal levels revealed a modest decrease of ∼15% in cells in S-phase of the cell cycle at the intermediate level, where palate fusion first occurs (P=0.017; Fig. 1G,I). Similarly, Moz-deleted E10.5 pharyngeal arch cells displayed a reduction in the percentage of cycling cells to ∼65% of controls, as assessed by flow cytometric analyses (P=0.03; not shown).

Loss of MOZ affects the expression of genes required for craniofacial development

$Moz^{-/-}$ pups have a range of craniofacial anomalies affecting the palate, the upper and the lower jaw. Cleft palate occurs with 100% penetrance (Voss et al., 2012). Development of the secondary palate begins with the outgrowth of palatal shelves as horizontal ridges on
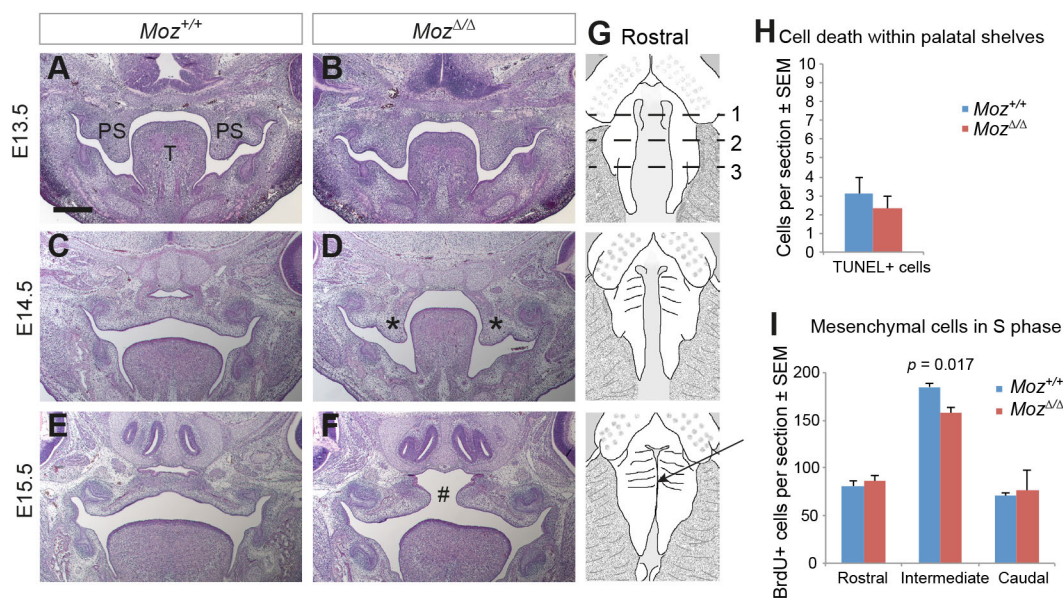

Fig. 1. In the absence of MOZ, palatal shelf elevation is delayed and fusion fails. (A-F) Hematoxylin and Eosin sections of $Moz^{+/+}$ and $Moz^{\Delta/\Delta}$ foetuses at E13.5, E14.5 and E15.5. (G) Schematic representation of the ventral view of the developing palate. Arrow indicates the site of first contact in palatal shelf fusion. (H) Enumeration of TUNEL-positive cells within palatal shelf sections at E13.5. (I) BrdU incorporation in the rostral, intermediate and caudal regions of the E13.5 palatal shelves (corresponding approximately to levels 1, 2 and 3 in G, respectively). PS, palatal shelf; T, tongue; asterisks indicate a delay in palatal shelf elevation; # indicates failure of palatal shelf fusion. n=3 animals per developmental stage and per genotype. Scale bar: 336 μm in A,B; 380 μm in C,D; 420 μm in E,F. Data are mean±s.e.m. and were analysed by one-way ANOVA with genotype as the independent factor followed by Bonferroni's post-hoc test (H,I).
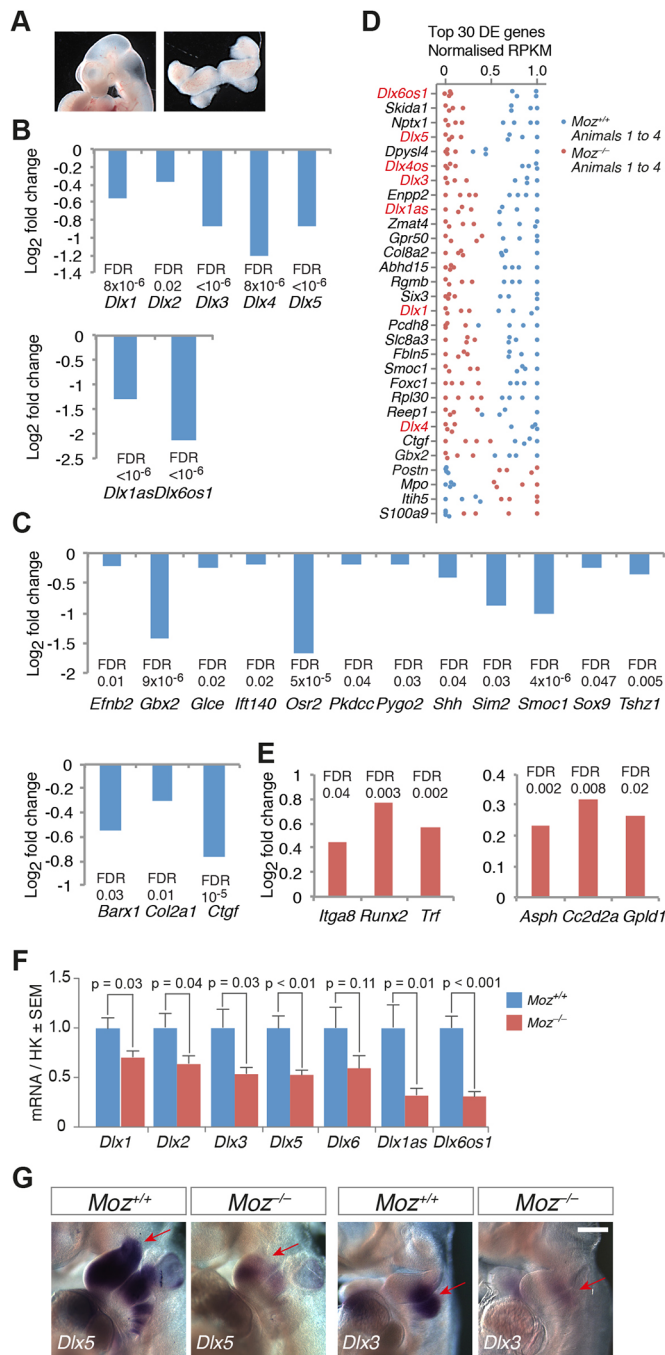
Fig. 2. Distal-less homeobox gene family expression is reduced in *Moz*^{–/–} embryos. (A) Tissue isolation of the maxillary and mandibular regions of E10.5 1st pharyngeal arch and 2nd pharyngeal arch for RNA-sequencing experiments. (B-E) Results of RNA-sequencing experiment comparing E10.5 *Moz*^{–/–} with *Moz*^{+/+} 1st and 2nd pharyngeal arch mRNA levels. (B,C,E) Log$_2$ fold-change between *Moz*^{–/–} and *Moz*^{+/+} samples of mRNA levels of genes required for palate development. (D) mRNA levels of the top 30 differentially expressed (DE) genes between individual *Moz*^{+/+} and *Moz*^{–/–} samples expressed as normalised RPKM (reads per kilobase per million reads). Dlx genes are in red. All DE genes and the corresponding *P* values and false discovery rates (FDR) corrected for transcriptome-wide significance are displayed in Table S1. RNA-seq reads in the *Moz* locus and RPKM values for selected genes in *Moz*^{+/+}, *Moz*^{+/–} and *Moz*^{–/–} are displayed in Fig. S1. RNA-seq data of *Moz*^{+/+} and *Moz*^{–/–} E13.5 palatal shelves are provided in Table S2 and Fig. S1. (F) RT-qPCR analysis of Dlx gene mRNA levels in E10.5 *Moz*^{+/+} and *Moz*^{–/–} 1st and 2nd pharyngeal arches independent from samples used in B-E, normalised to the housekeeping genes *Hsp90ab1*, *Pgk1* and *Rpl13*. RT-qPCR assessment of *Dlx1*, *Dlx2*, *Dlx5* and *Dlx6* in the maxillary region of the 1st pharyngeal arch specifically at E10.5 and E11.5, as well as in palatal shelves at E13.5 and E14.0 is shown in Fig. S3. (G) Whole-mount *in situ* hybridisation of E10.5 *Moz*^{+/+} and *Moz*^{–/–} embryos detecting *Dlx5* and *Dlx3* mRNA (purple stain). Arrows indicate first (*Dlx5*) and second (*Dlx3*) pharyngeal arches. Staining was stopped when wild-type control embryos showed the published expression pattern to reveal differences in expression levels. Endpoint staining to assess changes in the expression domains of *Dlx1*, *Dlx2, Dlx3, Dlx5, Dlx6* and *Dlx1as* are displayed in Fig. S2. *n*=4 animals per genotype in A-E, *n*=6 per genotype in F and *n*=12 per genotype in G. Scale bar: 230 μm in *Dlx5* images; 300 μm in *Dlx3* images. Data in B,C,E are presented as log$_2$ fold-change in *Moz*^{–/–} versus *Moz*^{+/+} or as normalised RPKM in D, and were analysed as described under RNA-seq analysis in the Materials and Methods. Data in F are presented as mean±s.e.m. and were analysed using two-tailed Student's *t*-test.

profiling (Fig. 2A). Among the more than 500 genes that were downregulated in the *Moz*^{–/–} 1st and 2nd pharyngeal arches (*P* values 0.002 to 6×10^{–22}; FDR<0.05; listed in Table S1) were 19 genes that had previously been associated with cleft palates [*Barx1*, *Col2a1*, *Ctgf* (*Ccn2*), *Dlx1*, *Dlx2*, *Dlx3*, *Dlx5*, *Efnb2*, *Gbx2*, *Glce*, *Ift140*, *Osr2*, *Pkdcc*, *Pygo2*, *Shh*, *Sim2*, *Smoc1*, *Sox9* and *Tshz1*; Fig. 2B,C]. Among these, the distal-less homeobox (Dlx) gene family stood out as five members of this family were affected by the loss of MOZ (*Dlx1*, *Dlx2*, *Dlx3*, *Dlx4*, *Dlx5*; *P* values 0.003 to 6×10^{–13}; FDR<0.05; Fig. 2B; Table S1). *Dlx1*, *Dlx3*, *Dlx4* and *Dlx5* were among the top 30 differentially expressed genes (Fig. 2D; *P* values and FDRs in Table S1). In addition to the Dlx genes, the gastrulation brain homeobox 2 (*Gbx2*) and odd-skipped related 2 (*Ors2*) genes were particularly affected by loss of MOZ (Fig. 2C). *Dlx1*, *Dlx3*, *Dlx4*, *Dlx5* and *Gbx2* mRNA levels in *Moz*^{+/–} heterozygous pharyngeal arches were intermediate between *Moz*^{–/–} and *Moz*^{+/+} (Fig. S1), suggesting a tight regulation of these genes by MOZ. Six genes that had previously been associated with cleft palates were upregulated in the *Moz*^{–/–} pharyngeal arches (*P* values 0.001 to 10^{–5}; FDR<0.05; Fig. 2E; Table S1). Among these, the runt-related transcription factor 2 gene (*Runx2*) was most prominently affected by loss of MOZ (Fig. 2E).

Based on their prominence among the top 30 differentially expressed genes, we investigated the effects of loss of MOZ on the Dlx gene family and downstream target genes of DLX transcription factors further.

The effects of loss of MOZ on Dlx gene family mRNA and antisense RNA levels were confirmed by RT-qPCR on independent E10.5 1st and 2nd pharyngeal arch samples (Fig. 2F). Together, the RNA-seq and RT-qPCR data showed that *Dlx1*, *Dlx2*, *Dlx3*, *Dlx4* and *Dlx5* gene expression was lower in *Moz*^{–/–} embryos compared with controls. However, it did not distinguish whether the mRNA levels were lower because the expression levels were lower or

the oral side of the maxillary part of the first pharyngeal arch between E10.5 and E11.5 in mouse development. We wanted to examine the effects of loss of MOZ on gene expression before palate development was initiated to avoid possible confounding effects of already changed tissue and cell type compositions in the samples, reasoning that any effects of MOZ on gene expression should be detectable prior to its effects on phenotypic outcome. We therefore began our investigation at E10.5.

To enrich for facial, maxillary and mandibular structures [while at the same time performing RNA-seq on a tissue type that would also provide enough material for chromatin immunoprecipitation (ChIP) experiments], we dissected the maxillary and mandibular component of the first pharyngeal arch, as well as the second pharyngeal arch at E10.5, and used these for RNA-seq expression

because the expression domains were smaller. To distinguish these two possibilities, we conducted whole-mount *in situ* hybridisation with a shorter (dynamic range; Fig. 2G) and a longer (endpoint; Fig. S2) staining to reveal expression levels and full expression domains, respectively. We observed that Dlx gene expression was impaired in both ways, the expression levels of *Dlx3* and *Dlx5* were lower (Fig. 2G), and the expression domains of *Dlx1*, *Dlx2*, *Dlx3*, *Dlx5* and *Dlx6* appeared reduced in size (Fig. S2).

To investigate the effects of MOZ for the duration of palate development, we dissected the maxillary component of the first pharyngeal arch, at E10.5 and E11.5, as well as the palatal shelves at E13.5 and E14.0, and determined Dlx gene expression levels by RT-qPCR. In addition, we conducted RNA-seq experiments on E13.5 palatal shelves. Overall, Dlx gene expression was lower in the *Moz*^{−/−} tissues than in controls (Fig. S3). These data indicate that normal levels of mRNA expression of the *Dlx1*, *Dlx2*, *Dlx3* and *Dlx5* genes depend on MOZ from the earliest stages of craniofacial and palate development, and that the importance of MOZ for *Dlx1* and *Dlx2* gene expression persists throughout palate development (Figs S1 and S3; Tables S1 and S2).

MOZ directly regulates the *Dlx5* locus
Homozygous mutation of *Dlx1* (Qiu et al., 1997), *Dlx2* (Qiu et al., 1995) or *Dlx5* (Acampora et al., 1999; Depew et al., 1999) causes cleft palate with different levels of penetrance; the highest penetrance results from loss of *Dlx5* on a mixed genetic background, which at 88% is similar to the penetrance of cleft palate in *Moz*-null pups on a mixed background (100%). Moreover, *Dlx5* gene expression was strongly affected by the absence of MOZ (Fig. 2B,F). To determine whether the *Dlx5* gene was likely to be a direct MOZ target, we examined MOZ occupancy and histone acetylation by chromatin immunoprecipitation (ChIP) followed by qPCR or sequencing. ChIP-qPCR of microdissected pharyngeal arches derived from embryos homozygous for a Flag-V5-BIO tag fused to the C-terminal end of MOZ (*Moz*^{V5/V5}; Vanyai et al., 2015) revealed enrichment for the MOZ-V5 signal in *Moz*^{V5/V5} at two sites within the *Dlx5* gene compared with wild-type controls (Fig. 3A,B). Histone 3 lysine 9 acetylation (H3K9ac) was reduced in the absence of MOZ (Fig. 3C). In contrast, H4K14ac was unaffected by *Moz* gene status (Fig. 3D). Furthermore, ChIP-seq experiments suggested further areas of enrichment of MOZ-V5 in the *Dlx5/Dlx6/Dlx6os* locus (Fig. 3E). ChIP-qPCR experiments confirmed three of these regions of enrichment (Fig. 3F). In comparison with the *Dlx5* locus, the *Dlx1*, *Dlx2*, *Dlx3* and *Dlx4* loci did not show similarly strong MOZ occupancy by ChIP-seq (not shown). However, owing to the small amount of input material (1st and 2nd pharyngeal arches), we cannot exclude the possibility that MOZ also occupies other Dlx genes at lower levels.
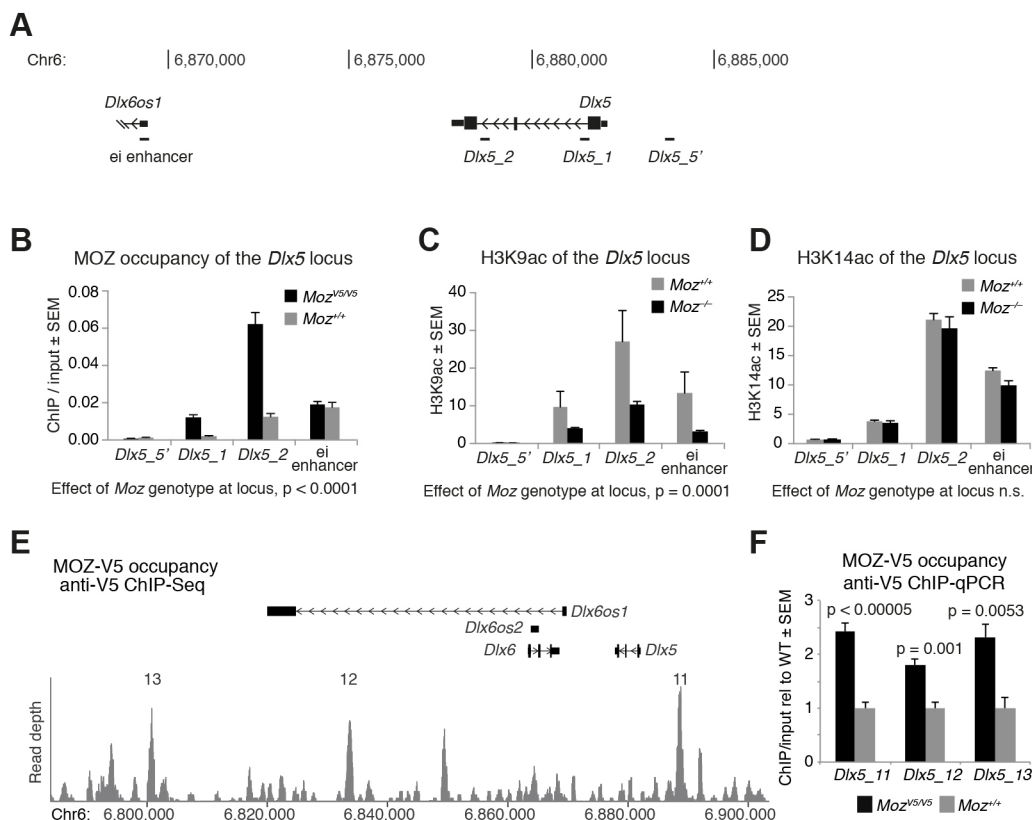

Fig. 3. *Dlx5* is a direct target of MOZ. (A) Schematic representation of the *Dlx5* locus, including the transcription start site of *Dlx6os1* in the ei enhancer. Sites amplified by qPCR following ChIP are indicated. (B) MOZ occupancy assessed using anti-V5 ChIP-qPCR of *Moz*^{V5/V5} knock-in compared with *Moz*^{+/+} microdissected first and second pharyngeal arches. In contrast to *Moz*^{−/−}, *Moz*^{V5/V5} knock-in mice produce intact MOZ protein and are viable, fertile and healthy. (C) Anti-H3K9ac ChIP-qPCR of E10.5 *Moz*^{+/+} and *Moz*^{−/−} pharyngeal arches. (D) Anti-H3K14ac ChIP-qPCR of E10.5 *Moz*^{+/+} and *Moz*^{−/−} pharyngeal arches. (E) Anti-V5 ChIP-seq read depth plot of a whole E10.5 *Moz*^{V5/V5} embryo. (F) Verification of major peaks indicated in E by ChIP-qPCR on separate whole E10.5 *Moz*^{V5/V5} versus *Moz*^{+/+} embryos. *n*=7 *Moz*^{V5/V5} and *n*=8 *Moz*^{+/+} (B), *n*=7 per genotype (C) and *n*=4 per genotype (D) pairs of microdissected first and second pharyngeal arches. *n*=5-6 *Moz*^{V5/V5} and *n*=4-6 *Moz*^{+/+} whole E10.5 embryos in F. Data are mean±s.e.m. and were analysed using three-way ANOVA with genotype, genomic site and experimental series as the independent factors, followed by Bonferroni's post-hoc test (B-D) or by two-tailed Student's *t*-test (F).

Absence of MOZ causes reduced expression of DLX target genes

A number of DLX transcription factor target genes, as well as regulatory pathways have been proposed as relevant to craniofacial development by previous studies (summarised in Fig. 4A). Expression of the zinc-finger transcription factor genes odd-skipped related 1 and 2 (*Osr1* and *Osr2*), the BarH-like homeobox gene 1 (*Barx1*), the forkhead box transcription factor gene *Foxl2*, the basic helix-loop-helix (bHLH) transcription factor single-minded homolog 2 gene (*Sim2*) and the POU domain transcription factor gene *Pou3f3* is reduced in $Dlx2^{-/-}$ and/or $Dlx1^{-/-};Dlx2^{-/-}$ mutant embryos (Jeong et al., 2012, 2008). Similarly, mRNA levels of the goosecoid homeobox gene (*Gsc*) and *Gbx2*, as well as the heart and neural crest derivatives expressed 2 gene (*Hand2*) are decreased in $Dlx5^{-/-}$ and/or $Dlx5^{-/-};Dlx6^{-/-}$ mutants (Depew et al., 1999, 2002; Jeong et al., 2008). Of these, *Gbx2* and *Hand2* have been confirmed as direct targets of DLX transcription factors (Barron et al., 2011; Jeong et al., 2008).

The expression of the DLX target genes *Osr1*, *Osr2*, *Gbx2*, *Sim2* and *Barx1* were significantly downregulated in the E10.5 $Moz^{-/-}$ pharyngeal arches RNA-seq data compared with $Moz^{+/+}$ controls (FDR 0.03 to 9×10^{-6}; Fig. S4; Table S1). Moreover, the expression of DLX transcription factor targets was also downregulated in $Moz^{-/-}$ mutants compared with $Moz^{+/+}$ embryos as assessed by whole-mount *in situ* hybridisation (*Hand2*, *Gbx2*, *Gsc*, *Osr2* and *Sim2*, Fig. 4; *Osr1* and *Pou3f3*, Fig. S5). In contrast, pituitary homeobox 2 (PITX2) has been implicated in the regulation of *Dlx2*, i.e. acting upstream of Dlx gene expression (Green et al., 2001; Venugopalan et al., 2011). Consistent with this, *Pitx2* expression in the pharyngeal arches was not affected by the loss of MOZ (Fig. S5). Similarly, other genes

reported to operate upstream of Dlx gene expression or at the same level were not differentially expressed (Fig. S4).

These data indicate that, along with *Dlx* gene expression, the mRNA levels of genes downstream of DLX transcription factors were also downregulated in the absence of MOZ, whereas upstream factors were not affected.

Differentiation genes are prematurely upregulated in the absence of MOZ

The palate is formed by intramembranous ossification from mesenchymal condensations (Bush and Jiang, 2012). During this process, mesenchymal cells under the influence of the transcription factors paired box 1 and 9 (PAX1 and PAX9), as well as NK3 homeobox 1 and 2 (NKX3-1 and NKX3-2) give rise to skeletal precursor cells that, in the presence of RUNX2, form osteoprogenitor cells and then osteoblasts (reviewed by Hartmann, 2009; Lefebvre and Bhattaram, 2010). In contrast, SRY-box 9 (SOX9) induces the formation of chondroblasts in regions of endochondral ossification from cartilage precursors. RUNX2 (Komori et al., 1997; Otto et al., 1997) and PAX9 (Peters et al., 1998) are essential for skeletal development. PAX9 induces the differentiation of mesenchymal cells to bipotential skeletal precursor cells, and RUNX2 supports differentiation towards the osteoblast lineage.

Apart from the downregulation of genes required for palate development, the $Moz^{-/-}$ E10.5 pharyngeal arches displayed an upregulation of genes involved in osteoblast differentiation. *Runx2* and *Nkx3-1* were upregulated (Fig. S6; Table S1). Bone collagen genes *Col6a1* and *Col6a3* were upregulated in $Moz^{-/-}$ E10.5 pharyngeal arches. Furthermore, the osteoblast-specific factor/ periostin gene (*Postn*) was upregulated. In contrast, *Sox9* and the
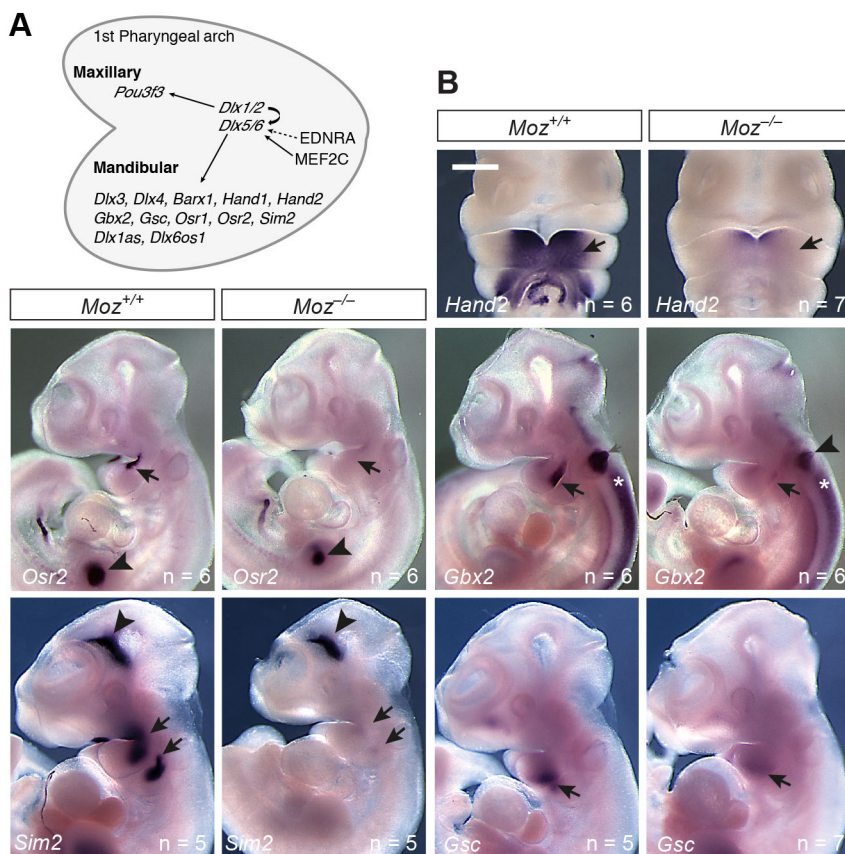

Fig. 4. Loss of MOZ affects the gene network downstream of DLX transcription factors. (A) Simplified schematic representation of DLX transcription factors and their (direct or indirect) downstream targets. Arrows indicate activation, dashed arrows indicate known indirect activation (based on data from Charite et al., 2001; Jeong et al., 2012, 2008; Verzi et al., 2007). (B) Whole-mount *in situ* hybridisation of E10.5 $Moz^{+/+}$ and $Moz^{-/-}$ embryos for genes downstream of DLX transcription factors. Arrows indicate pharyngeal arch expression domains that are affected by the loss of MOZ. Arrowheads indicate expression domains outside the pharyngeal arches; asterisks indicate neural tube expression domains. *n* values are as indicated. Scale bar: 550 µm. Quantitative assessment by RNA-sequencing of these and further DLX target genes are displayed in Fig. S4 and Table S1, and whole-mount *in situ* hybridisation of further DLX target genes are in Fig. S5.

SOX9 target genes encoding cartilage collagens, *Col2a1* and *Col9a1*, were downregulated. A similar pattern was observed in the *Moz*^{−/−} E13.5 palatal shelves, where the bone collagen gene *Col1a2* was upregulated (Fig. S6; Table S2), which is a RUNX2 target gene (Kern et al., 2001). At E13.5, additional genes promoting bone formation and encoding bone matrix proteins were upregulated in the *Moz*^{−/−} palatal shelves. These included genes encoding elements of the bone morphogenetic protein (BMP) and transforming growth factor β (TGFβ) signalling pathways [BMP5, ALK1/ACVRL1 (activin A receptor-like type 1), TGFB2], as well as the matrix-associated secreted protein acidic and cysteine-rich protein (SPARC; Fig. S6; Table S2). The upregulation of genes that promote osteogenesis and of bone collagen genes suggests that the *Moz*^{−/−} E10.5 pharyngeal arches and E13.5 palatal shelves may undergo premature osteoblast lineage differentiation.

MOZ is required cell-autonomously for the expression of Dlx genes

The bulk of the cells expressing Dlx genes in the pharyngeal arches are neural crest cells. An ability of MOZ to directly activate one or more of the Dlx gene family loci would necessitate a cell-autonomous requirement for MOZ within the neural crest for Dlx gene expression. To test this requirement, we used a *Wnt1* promoter-driven cre-recombinase transgene [*Wnt1-cre*[T] (Danielian et al., 1998)] to delete the *loxP*-flanked exons 3 to 7 of the *Moz* conditional mutant allele (*Moz*[lox]) in the neural ectoderm, which gives rise to the neural crest cells that migrate to the pharyngeal arches.

Deletion of *Moz* in the *Wnt1-cre* lineage (*Moz*[lox/lox];*Wnt1-cre*[T/+]) resulted in neonatal lethality (data not shown), leading to underrepresentation at weaning (Fig. 5A). Gross examination, skeletal preparations and serial sectioning (Fig. 5B, Fig. S7, Table S3) of E18.5 heads revealed cleft of the soft palate in 10 of 10 *Moz*[lox/lox];*Wnt1-cre*[T/+] pups, which was never seen in control *Moz*^{+/+}; *Wnt1-cre*[T/+] animals. An abnormal additional bone caudal to the alisphenoid bone (similar to the os paradoxicum observed in *Dlx5* null mice) was observed in 4 of 4 *Moz*[lox/lox];*Wnt1-cre*[T/+] animals examined for its presence.

All except one *Moz*[lox/lox];*Wnt1-cre*[T/+] pup displayed a normal external appearance. Only this one severely affected *Moz*[lox/lox]; *Wnt1-cre*[T/+] pup displayed shortening of the upper and lower jaw (Fig. S7). RT-qPCR analysis of E10.5 pairs of microdissected first and second pharyngeal arches confirmed that loss of MOZ in the neural crest resulted in the downregulation of Dlx genes compared with control samples (Fig. 5C) to levels similar to those observed in *Moz* germline-deleted (*Moz*^{−/−}) pharyngeal arches (Fig. 2F).

Genetic interaction between the Moz and Dlx5 loci

Dlx5 homozygous mutant animals have numerous craniofacial defects (Acampora et al., 1999; Depew et al., 1999, 2005; Han et al., 2009), which appear to vary depending on the genetic background and include cleft of only the soft palate (Han et al., 2009) or the bony palate (88%) (Acampora et al., 1999; Depew et al., 1999), and asymmetric hypoplasia (88%) or near-complete agenesis of the nasal capsule and cavity (Depew et al., 1999). In addition to these defects, *Dlx5*^{−/−} mutants have an ectopic bone structure originating from the ectotympanic process and extending toward the pterygoid process, termed the os paradoxicum (Acampora et al., 1999; Depew et al., 1999).

As our results thus far suggested that the Dlx gene family requires MOZ for normal mRNA expression levels in E10.5 embryos and that the *Dlx5* locus was directly activated by MOZ, genetic
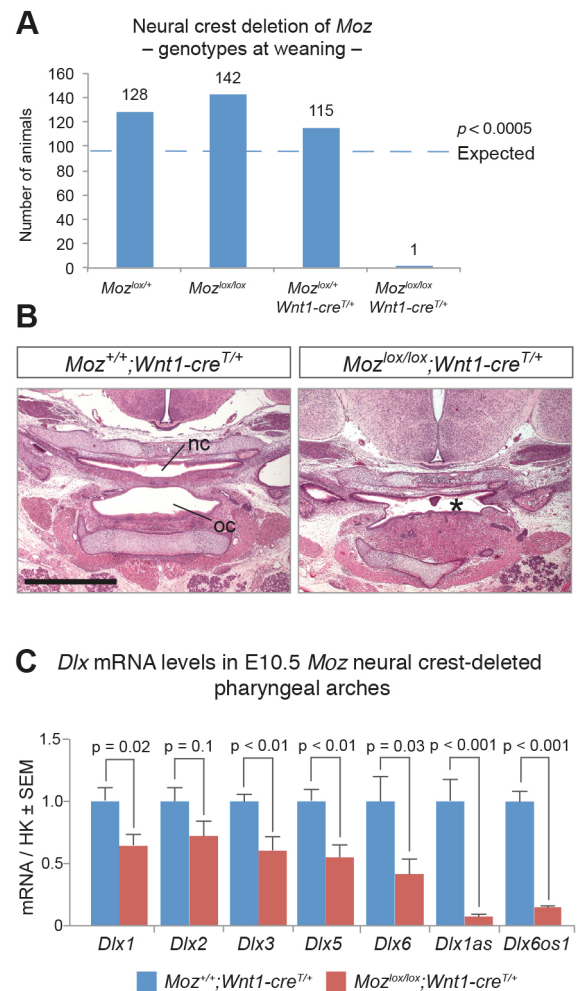
A Neural crest deletion of *Moz* – genotypes at weaning –

B

C *Dlx* mRNA levels in E10.5 *Moz* neural crest-deleted pharyngeal arches

Fig. 5. A cell-autonomous requirement for MOZ in neural crest cells. (A) Survival at weaning (3 weeks of age) of offspring from *Moz*[lox/lox] by *Moz*[lox/+]; *Wnt1-cre*[T/+] matings. The *Wnt1*-driven cre-recombinase deletes *Moz* in neuroepithelium that gives rise to the neural crest. (B) Hematoxylin and Eosin stained frontal sections of E18.5 *Moz*^{+/+};*Wnt1-cre*[T/+] and *Moz*[lox/lox];*Wnt1-cre*[T/+] heads at the level of the soft palate. The intact soft palate in the control separates the nasal cavity (nc) from the oral cavity (oc). The cleft of the *Moz*[lox/lox];*Wnt1-Cre*[T/+] soft palate is indicated by an asterisk. Serial sections were examined. (C) RT-qPCR analysis of *Dlx* mRNA levels in microdissected sets of E10.5 first and second pharyngeal arches normalised to the housekeeping genes *Hsp90ab1*, *Pgk1* and *Rpl13* with and without neural crest-specific deletion of *Moz*. Scale bar: 1 mm in B. Data are total counts of animals (A) or mean±s.e.m. (C), and were analysed by Fisher's exact test (A) or two-tailed Student's *t*-test (C). *n* is as indicated in A, *n*=3 *Moz*[lox/lox];*Wnt1-cre*[T/+] and *n*=3 *Moz*^{+/+};*Wnt1-cre*[T/+] controls in B and *n*=6 per genotype in C. Further data are shown in Fig. S7 and Table S3.

interaction between the *Moz* and *Dlx5* genes was examined in the offspring of *Moz*^{+/−} by *Dlx5*^{+/−} matings. *Moz*^{+/−}; *Dlx5*^{+/−} animals were underrepresented at weaning (3 weeks of age; Fig. 6A), indicating synergy between *Moz* and *Dlx5* heterozygosity. Analysis of pups revealed that 11 out of 17 *Moz*^{+/−};*Dlx5*^{+/−} animals had a cleft of the soft palate, which was not observed in wild type or either single heterozygous animals (asterisk in Fig. 6F), but similar to the cleft soft palate produced through *Wnt1*-Cre mediated deletion of *Moz* (see overview in Table S3). Although clefts of the soft and/or bony palate were a common feature of *Moz*^{−/−};*Dlx5*^{−/−} and *Moz*^{+/−}; *Dlx5*^{+/−} pups, *Moz*^{+/−};*Dlx5*^{+/−} pups displayed certain similarities with *Dlx5*^{−/−} animals that were not present in *Moz*^{−/−} animals.
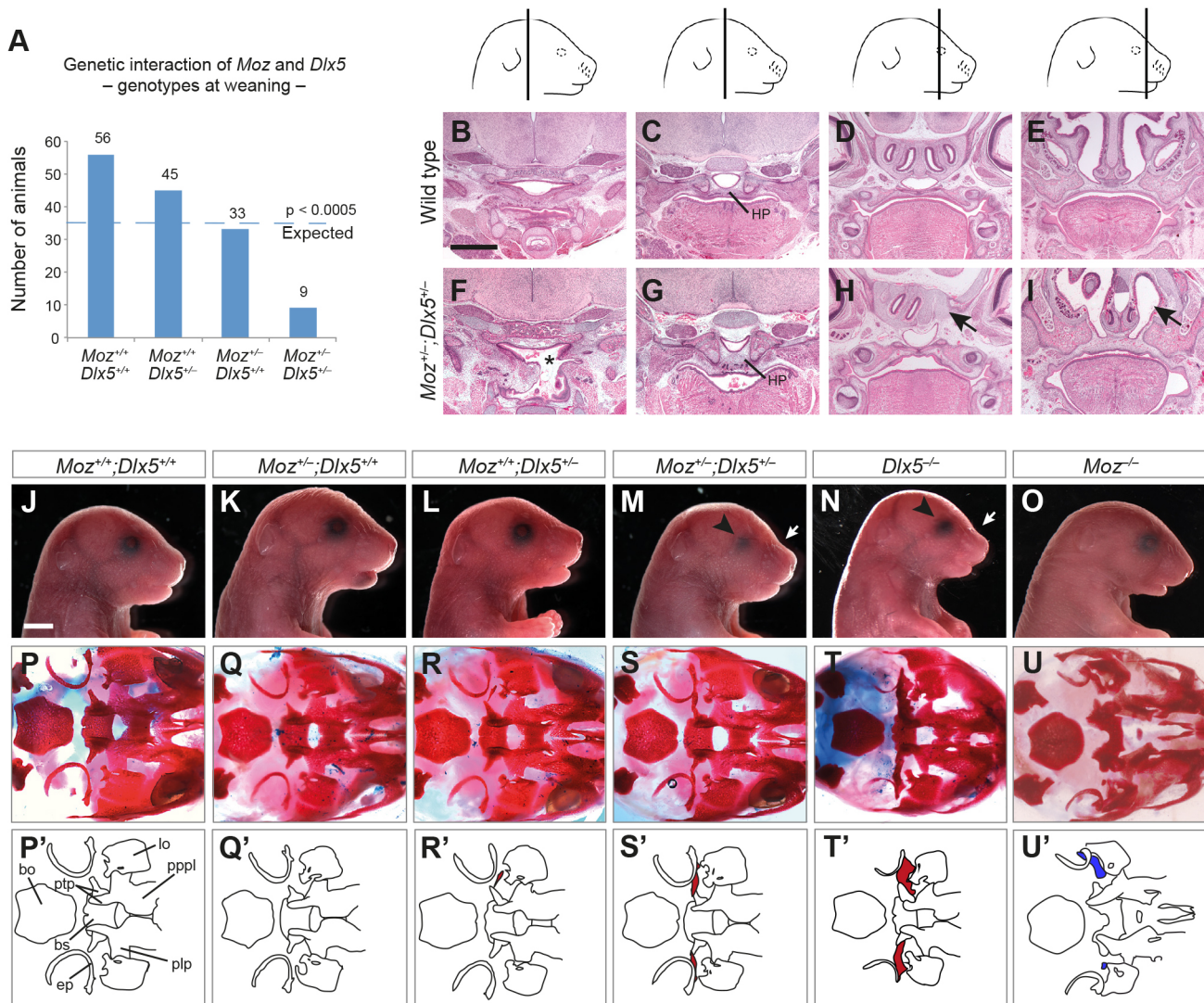
Fig. 6. Genetic interaction between *Moz* and *Dlx5*. (A) Survival at weaning (3 weeks of age) of offspring from *Moz⁺/⁻* by *Dlx5⁺/⁻* matings. (B-I) Frontal Hematoxylin and Eosin stained sections of the head displaying the nasal cavity, palate and mouth cavity of *Moz⁺/⁻;Dlx5⁺/⁻* and wild-type E18.5 foetuses at the rostro-caudal levels indicated schematically above. Asterisk indicates a cleft of the *Moz⁺/⁻;Dlx5⁺/⁻* soft palate. In addition, *Moz⁺/⁻;Dlx5⁺/⁻* show a thickened hard palate (HP in G) and asymmetric hypoplasia of the nasal capsule and nasal septum (arrows in H,I). Serial sections were examined. (J-O) Lateral view of E18.5 heads. Genotypes are as indicated. *Moz⁺/⁻;Dlx5⁺/⁻* double heterozygous mutants display microphthalmia (2/12; arrowhead, M) and depression in the dorsal surface of the rostrum (3/14; arrow, M), similar to *Dlx5⁻/⁻* pups (N). Representative images are shown. (P-U) Ventral view of skull, lower jaw removed. (P'-U') Schematic diagrams of the caudal half of this area. All *Moz⁺/⁻;Dlx5⁺/⁻* double heterozygous animals displayed an ectopic ossified strut, the os paradoxicum (red segments, S'), extending medially from the ectotympanic process (ep) toward the pterygoid process (ptp), which is present and more extensively ossified in *Dlx5⁻/⁻* animals (red segments, T'). *Moz*-deleted pups occasionally show an additional bone in a similar location (blue segments, U'). No similar structure was found in wild-type, *Moz⁺/⁻;Dlx5⁺/⁺* or *Moz⁺/⁺;Dlx5⁺/⁻* single heterozygous animals, except for a small fragment of ectopic bone in 1 out of 6 *Moz⁺/⁺; Dlx5⁺/⁻* single heterozygotes. Images of the lower jaws are displayed in Fig. S8. bo, basioccipital bone; bs, basisphenoid bone; ep, ectotympanic process; lo, lamina obturans; plp, palatine process; pppl, palatal process of palatine bone; ptp, pterygoid process. Scale bars: in B, 820 µm for B-I; in J, 3 mm for J-O and 1.2 mm for P-U. Data are total counts of animals (A) and were analysed using Fisher's exact test (A). *n* is as indicated in A, *n*=3 *Moz⁺/⁺;Dlx5⁺/⁺* controls and *n*=14 *Moz⁺/⁻;Dlx5⁺/⁻* animals in B-I, and *n*=7 *Moz⁺/⁺;Dlx5⁺/⁺*, *n*=6 *Moz⁺/⁻;Dlx5⁺/⁺*, *n*=6 *Moz⁺/⁺;Dlx5⁺/⁻*, *n*=14 *Moz⁺/⁻;Dlx5⁺/⁻*, *n*=5 *Dlx5⁻/⁻*, *n*=3 *Moz⁻/⁻* and *n*=6 *Moz^(Δ/Δ)* animals in P-U. Further data are provided in Table S3.

Asymmetric hypoplasia of the nasal capsules was observed in *Moz⁺/⁻; Dlx5⁺/⁻* (arrows in Fig. 6H,I) and *Dlx5⁻/⁻* pups, but not in *Moz⁻/⁻* animals. Externally, a depression in the dorsal surface of the rostrum reminiscent of *Dlx5⁻/⁻* pups was observed in three out of 14 *Moz⁺/⁻; Dlx5⁺/⁻* pups. This depression was not observed in wild-type, *Moz⁻/⁻* or single heterozygous animals (arrows Fig. 6M,N).

Analysis of skeletal preparations of wild-type, *Moz⁺/⁻*, *Dlx5⁺/⁻*, *Moz⁺/⁻;Dlx5⁺/⁻*, *Moz⁻/⁻* and *Dlx5⁻/⁻* E18.5 pups revealed an ossified strut in all six *Moz⁺/⁻;Dlx5⁺/⁻* pups examined, albeit less extensive than the os paradoxicum observed in *Dlx5⁻/⁻* mutants (indicated in

red in Fig. 6S',T', Table S3). This ectopic bone was not observed in any wild-type or *Moz* single heterozygous animal, whereas one out of six *Dlx5⁺/⁻* single heterozygous pups had a very small fragment of ectopic bone in approximately the same region (indicated in red in Fig. 6R'). *Moz*-deficient pups occasionally had a supernumerary bone structure in a similar position (indicated in blue in Fig. 6U'). Lastly, *Moz⁺/⁻;Dlx5⁺/⁻* animals, and animals that had lost one or both copies of the *Dlx5* gene or the *Moz* gene displayed varying degrees of shortening of the mandible, as well as a shortening of individual bony protrusions from the mandible (Fig. S8).

Effects of *Moz* and *Dlx5* heterozygosity on gene transcription
In order to determine whether the synergistic effects of the combined loss of *Moz* and *Dlx5* alleles extended to transcriptional regulation, we performed RNA-seq of microdissected first and second pharyngeal arches from individual stage-matched female E10.5 embryos of the following six genotypes: wild type, *Moz*$^{+/-}$, *Dlx5*$^{+/-}$, *Moz*$^{+/-}$;*Dlx5*$^{+/-}$, *Moz*$^{-/-}$ and *Dlx5*$^{-/-}$ (Fig. 7A). A greater-

than-additive increase in the number of up- and downregulated genes in *Moz*$^{+/-}$;*Dlx5*$^{+/-}$ tissues compared with the sum of each of the heterozygotes suggested synergy between the *Moz* and *Dlx5* genes in transcriptional regulation (Fig. 7B). *Dlx3* and *Dlx4* mRNA levels were downregulated in animals that had lost one of two copies of *Moz* and/or *Dlx5* (Fig. 7C; FDRs in Table S4; all differentially expressed genes in Table S5; Fig. S9). In *Dlx5*$^{-/-}$ mutant mice,
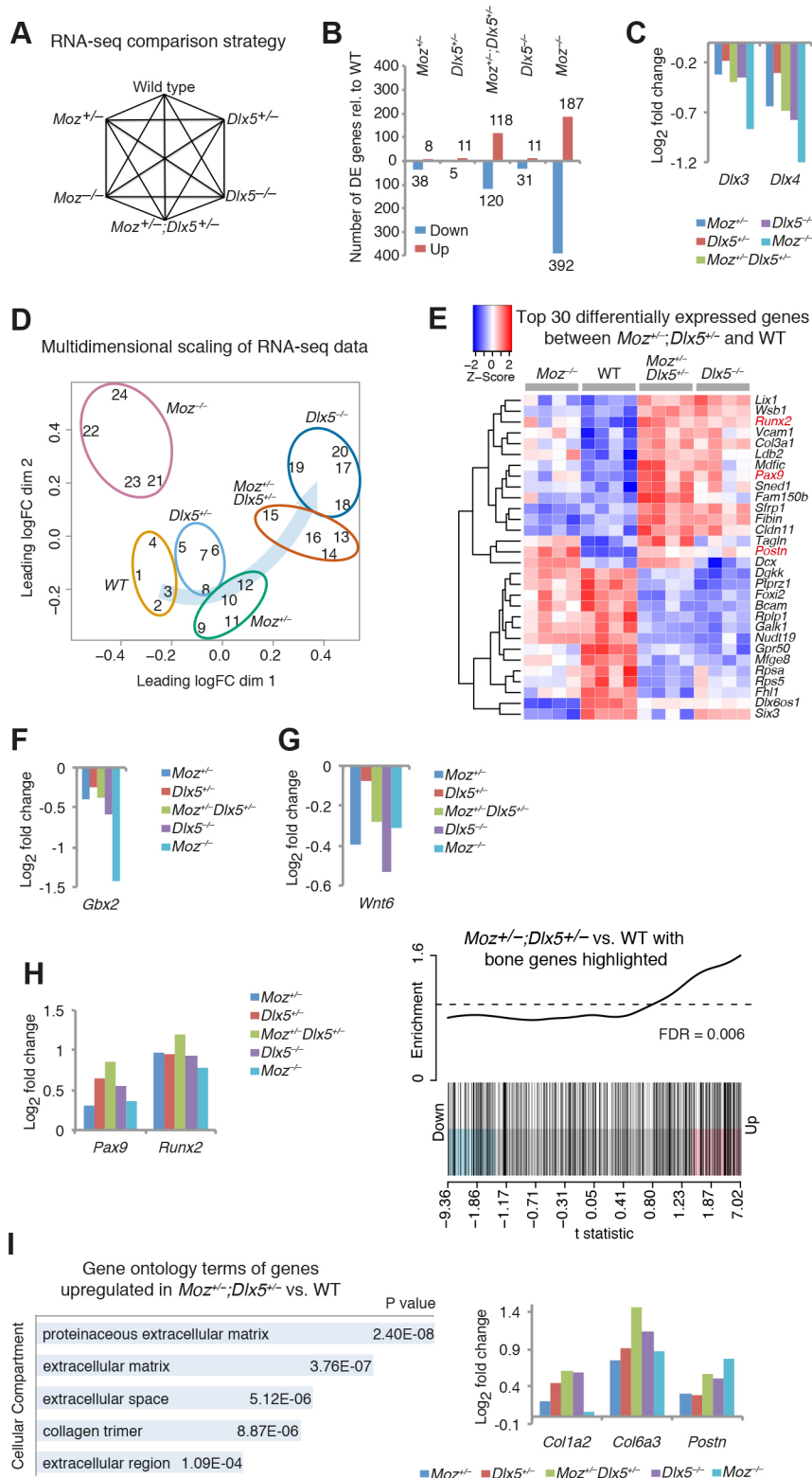

Fig. 7. Effects of single and compound loss of *Moz* and *Dlx5* on the pharyngeal arch transcriptome. (A) Strategy for the RNA-sequencing experiments comparing E10.5 1st and 2nd pharyngeal arches of wild type, *Moz*$^{+/-}$, *Dlx5*$^{+/-}$, *Moz*$^{+/-}$;*Dlx5*$^{+/-}$ double heterozygotes, *Dlx5*$^{-/-}$ and *Moz*$^{-/-}$. Differentially expressed (DE) genes are listed with FDRs in Tables S4 and S5. (B) Enumeration and direction of DE genes. (C) Log$_2$ fold-change in *Dlx3* and *Dlx4* mRNA levels in the *Moz* and/or *Dlx5* mutant samples relative to wild-type control. RNA-seq reads in the *Dlx5* locus and log$_2$ fold-changes of other Dlx genes are displayed in Fig. S9. (D) Multidimensional scaling plot showing distances between transcriptional profiles. Each RNA sample is represented by its sample number, genotypes are indicated. Distances on the plot represent 'leading log$_2$ fold-change' between each pair of samples. Blue arrow indicates direction of increasing similarity to *Dlx5*$^{-/-}$ embryos. (E) Heatmap of the top 30 genes most differentially expressed between *Moz*$^{+/-}$;*Dlx5*$^{+/-}$ and wild-type controls. Heatmaps of the contrast between *Dlx5*$^{-/-}$ and wild type, as well as *Moz*$^{-/-}$ and wild-type controls are displayed in Fig. S9. (F) Log$_2$ fold-change of mRNA levels of a confirmed target gene of DLX5. FDRs are displayed in Table S4. (G) Log$_2$ fold-change of mRNA levels of a gene encoding a promoter of proliferation of palatal mesenchymal cells (also see Fig. S6). FDRs are displayed in Table S4. (H) Log$_2$ fold-change of mRNA levels of genes encoding proteins promoting bone development and barcode plot showing upregulation of bone development-associated genes in *Moz*$^{+/-}$;*Dlx5*$^{+/-}$ animals relative to wild type. Genes are ordered left to right by differential expression t-statistic comparing *Moz*$^{+/-}$;*Dlx5*$^{+/-}$ with wild type. Vertical bars show positions of bone genes and 'worm' shows relative enrichment. Barcode plots for other genotypes are displayed in Fig. S9. FDRs are displayed in Table S4. (I) Cellular component gene ontology terms overrepresented in genes upregulated in *Moz*$^{+/-}$;*Dlx5*$^{+/-}$ compared with wild-type samples (horizontal axis shows adjusted *P*-value) and log$_2$ fold-change of mRNA levels of genes encoding bone-specific collagens and periostin. FDRs are displayed in Table S4. All data shown are from *n*=4 female E10.5 embryos for each of the six genotypes. Data were analysed as described under RNA-sequencing analysis.

where exons 1 and 2 are deleted, the *Dlx5* locus demonstrated substantial reads in the third exon, but negligible reads in exons 1 and 2 (Fig. S9). The other genotypes showed decreased numbers of reads in exons 1 and 2 to varying magnitudes when compared with wild type, with *Moz*$^{-/-}$ and *Moz*$^{+/-}$;*Dlx5*$^{+/-}$ showing the lowest number and *Dlx5*$^{+/-}$ expression intermediate between wild type and these genotypes. Most Dlx gene mRNA levels were also reduced in the *Dlx5*$^{-/-}$ and the *Moz*$^{+/-}$;*Dlx5*$^{+/-}$ pharyngeal arches (Fig. S9; FDRs in Table S4).

A multiple dimension scaling (MDS) plot showed that the biological replicates of each genotype clustered together (Fig. 7D). In addition, wild-type and single heterozygous samples grouped together. Interestingly, *Moz*$^{+/-}$;*Dlx5*$^{+/-}$ samples displayed expression profiles more similar to *Dlx5*$^{-/-}$ mutants when compared with either single heterozygote, indicating that loss of one allele of *Moz* shifted the expression profile of *Dlx5*$^{+/-}$ samples to become more *Dlx5*$^{-/-}$ mutant like. Overall, the MDS plot suggests a progression in transcriptional distance from wild type to single heterozygous mutants to double heterozygous mutants and finally to *Dlx5*$^{-/-}$ homozygous mutants, with the *Moz*$^{-/-}$ homozygous mutant expression profiles being separate and unlike the other genotypes (Fig. 7D).

A heatmap of the top 30 differentially expressed genes in *Moz*$^{+/-}$;*Dlx5*$^{+/-}$ samples compared with wild type showed that the *Moz*$^{+/-}$;*Dlx5*$^{+/-}$ resembled the *Dlx5*$^{-/-}$ patterns more closely than the *Moz*$^{-/-}$ and wild-type patterns (Fig. 7E). Correspondingly, a heatmap of the top 30 differentially expressed genes in *Dlx5*$^{-/-}$ samples compared to wild type also showed the similarity between the *Moz*$^{+/-}$;*Dlx5*$^{+/-}$ pattern and the *Dlx5*$^{-/-}$ samples (Fig. S9). In contrast, a heatmap of the top 30 differentially expressed genes in *Moz*$^{-/-}$ samples compared with wild type displayed a pattern for *Moz*$^{-/-}$ that was distinct from the other genotypes, as expected because MOZ directly regulates more genes than *Dlx5* alone (Figs 2, 7B; Tables S1 and S2). Even so, many genes in *Moz*$^{+/-}$;*Dlx5*$^{+/-}$ and *Dlx5*$^{-/-}$ samples showed changes in the same direction as the *Moz*$^{-/-}$ samples (Fig. S9).

The confirmed direct DLX transcription factor target gene *Gbx2* was downregulated in the *Moz* and/or *Dlx5* mutant genotypes (Fig. 7F; FDRs in Table S4). In contrast, the mRNA levels of upstream regulators of Dlx gene expression were not significantly affected, including the endothelin receptor type A (*Ednra*), fibroblast growth factor 8 (*Fgf8*), myocyte enhancer factor 2C (*Mef2c*) and Pitx2 genes (FDRs in Table S4).

The wingless-like protein 6 (*Wnt6*), a gene encoding a growth factor promoting the self-renewal of palatal mesenchymal cells (Jiang et al., 2017), was downregulated in *Moz* and/or *Dlx5* mutant genotypes compared with the wild-type controls (Fig. 7G; FDRs in Table S4). In contrast, bone development-inducing genes were upregulated in the *Moz*$^{+/-}$;*Dlx5*$^{+/-}$ and the *Dlx5*$^{-/-}$ samples compared with wild-type controls (Fig. 7H; Fig. S9). In particular, *Runx2* and *Pax9* mRNA were elevated in *Moz* and/or *Dlx5* mutant genotypes compared with the wild-type controls (Fig. 7H; FDRs in Table S4). Moreover, genes encoding proteinaceous extracellular matrix, including collagens, were significantly upregulated in the *Moz*$^{+/-}$;*Dlx5*$^{+/-}$ samples compared with wild-type controls (Fig. 7I). These included the bone-specific type I and type VI collagen genes [*Col1a2* (a RUNX2 target gene; Kern et al., 2001) and *Col6a3*], and the osteoblast-specific factor periostin (*Postn*; Fig. 7I; FDRs in Table S4). In particular, with respect to expression changes in *Runx2*, *Pax9*, *Col1a2*, *Col6a3* and *Postn*, loss of *Moz* and *Dlx5* appeared to synergise (Fig. 7H,I; Table S4), in that single knockouts had a lesser effect than loss of

one allele of both *Moz* and *Dlx5*. Overall, the expression profiles suggested premature onset of osteoblast differentiation in *Dlx5*, *Moz* and *Dlx5;Moz* compound mutant embryos.

DISCUSSION

Heterozygous mutation of the human *MOZ* (*KAT6A*) gene causes facial dysmorphogenesis and can result in palate defects (Arboleda et al., 2015; Millan et al., 2016; Tham et al., 2015) and homozygous deletion of *Moz* in mice causes cleft palate with 100% penetrance, indicating that MOZ is important for craniofacial development in humans and mice. In this study, we have identified the molecular mechanism of MOZ function during craniofacial development. Of a large number of genes affected by the lack of MOZ, we examined the distal-less homeobox genes, because seven of the top 30 differentially expressed genes were Dlx genes or their antisense RNAs, making them the most prominently affected gene family with reduced expression in the *Moz*-deleted embryos. Moreover, downstream target genes of DLX transcription factors were also affected. Genomic occupancy of the *Dlx5/Dlx6* locus by MOZ, tissue-specific deletion in the neural crest cells and genetic interaction between *Moz* and *Dlx5* indicated a direct effect of MOZ on *Dlx5* gene expression. MOZ is one of only a few chromatin modifiers implicated in palate and craniofacial development, and therefore joins the ranks of candidates proposed to account for the integration of genetic and environmental effects on this process. In this context, it should be noted that *Moz*$^{+/-}$ heterozygous mice are more susceptible to cleft palate caused by excessive supply of retinoic acid (Voss et al., 2012), suggesting that two wild-type alleles of *Moz* render palate development more robust.

Interestingly, the methyl-CpG-binding protein 2 has been found to recruit histone deacetylase 1 (HDAC1) to the *Dlx5/Dlx6* locus, promoting the repressive mark H3K9 methylation, at least in the brain (Horike et al., 2005). If this was also the case in craniofacial structures, *Dlx5/Dlx6* locus gene expression in craniofacial development may be regulated by the opposing functions of MOZ and HDAC1.

The DLX transcription factors are crucial for craniofacial development (Acampora et al., 1999; Depew et al., 1999, 2005; Jeong et al., 2012, 2008; Qiu et al., 1997, 1995). One-third of individuals with copy number variation at the *DLX5/DLX6* locus present with mild to severe palatal abnormalities, such as high palate or cleft palate and cleft lip (Elliott and Evans, 2006), and a *DLX4* mutation has been described in a child with bilateral cleft lip and palate (Wu et al., 2015). Single homozygous mutant mice for *Dlx1*, *Dlx2* and *Dlx5* display cleft palate with varying penetrance (Acampora et al., 1999; Depew et al., 1999, 2005; Han et al., 2009; Qiu et al., 1997, 1995).

Loss of MOZ causes a reduction in *Dlx1*, *Dlx2*, *Dlx3*, *Dlx4*, *Dlx5* and *Dlx6* mRNA levels by 25% to 55% (rather than complete loss). Compound heterozygous loss of *Dlx1*, *Dlx2*, *Dlx3*, *Dlx5* and *Dlx6* causes cleft palate with 100% penetrance (Depew et al., 2005). Although Depew and colleagues did not present the expression levels of the Dlx genes in the compound heterozygous mice, based on studies of other genes in which mRNA levels in heterozygous mice have been determined, it can be hypothesised that mRNA levels may be halved in the *Dlx1*, *Dlx2*, *Dlx3*, *Dlx5* and *Dlx6* compound heterozygotes. These levels are similar to those in the *Moz*-null embryos and represent limiting levels of Dlx gene mRNA. Although the effects of MOZ on the Dlx gene family alone could account for the complete penetrance cleft palate phenotype, direct effects of MOZ on other genes may also contribute to the cleft palate phenotype. The downregulation of 15 cleft palate genes in addition

to the Dlx genes in the *Moz*-null embryos would be expected to contribute to the *Moz*-null phenotype.

Supporting a role for MOZ in promoting transcription of Dlx genes, we found that loss of MOZ also affected the expression of target genes of DLX transcription factors, *Hand2* (Depew et al., 2002), *Gsc* (Depew et al., 1999), *Gbx2* (Jeong et al., 2008), *Osr1*, *Osr2* and *Sim2* (Jeong et al., 2012). The fact that the *Wnt1-cre* deletion of *Moz* caused a less severe phenotype than germline deletion suggests a role for MOZ outside the neural crest, in addition to the pronounced effects on Dlx gene expression within the neural crest. A role for MOZ in the epithelium remains to be examined. In contrast, mesoderm-specific deletion of *Moz* does not result in cleft palate or other craniofacial anomalies (Vanyai et al., 2015).

Mesenchymal cells of neural crest or mesodermal origin (reviewed by Lefebvre and Bhattaram, 2010) give rise to skeletal mesenchymal precursor cells (also termed osteochondral progenitors) under the influence of PAX9, NKX3-1 and other transcription factors (reviewed by Hartmann, 2009). Skeletal precursors can undergo self-renewing divisions and give rise to either chondrocytes or osteoblasts directed by opposing functions of SOX9 or RUNX2, respectively (Zhou et al., 2006). While RUNX2 is required for the differentiation of both chondrocytes and osteoblasts (Ducy et al., 1997; Komori et al., 1997; Otto et al., 1997; Stricker et al., 2002), it is considered a 'master regulator' of intramembraneous ossification (Bhatt et al., 2013; Takarada et al., 2016).

Genetic deletion of *Runx2* results in the complete failure of ossification (Komori et al., 1997; Otto et al., 1997); the combined absence of NKX3-1 and the related NKX3-2 causes skeletal anomalies, in particular in the cranial region (Herbrand et al., 2002), and the lack of PAX9 results in multiple skeletal defects, including cleft palate (Peters et al., 1998). *Runx2*, *Nkx3-1*, *Pax9* and bone-specific downstream effector genes were upregulated in *Moz*−/− single knockout, *Dlx5*−/− single knockout and *Moz*+/−;*Dlx5*+/− double heterozygous embryos. Upregulated collagen genes, *Col1a1*, *Col6a1* and *Col6a3*, encode structural proteins expressed during osteogenesis (Shoulders and Raines, 2009). Both neural crest- and mesoderm-derived cells produce a collagen-rich matrix in the early condensation state of skeletal development (reviewed by Lefebvre and Bhattaram, 2010). Several collagen genes, including *Col1a2*, *Col3a1* (Diez-Roux et al., 2011) and *Col6a2* (Reymond et al., 2002) are expressed during palate development. Mutations in human or mouse collagen genes, including *COL1A2* (Garofalo et al., 1991) and *COL2A1* (Snead and Yates, 1999), cause cleft palate. Collagen genes are directly regulated by SOX9 (Lefebvre et al., 1997) and DLX5 (Hojo et al., 2016), and by RUNX2 (Kern et al., 2001).

The downregulation of the gene encoding WNT6, which promotes palatal mesenchymal cell proliferation, and the modest reduction in cell proliferation combined with the upregulation of the bone differentiation-inducing genes *Pax9* and *Runx2*, as well as the bone extracellular matrix genes *Col1a2*, *Col6a3* and *Postn* in the *Moz* mutants and in the *Moz* and *Dlx5* compound mutants suggest a gradual premature cell cycle deceleration and premature onset of osteogenic lineage differentiation. Premature cell cycle deceleration and premature onset of differentiation would be expected to result in undersized palatal shelves that cannot meet and fuse in the midline, as observed in the *Moz*−/− embryos.

Cleft palate can occur as an intrinsic effect of palate development or as a consequence of other craniofacial anomalies. *Moz*-deficient mice display mild craniofacial defects, which may contribute to the cleft palate. The regulation of the *Dlx5* locus by MOZ may direct attention to the derivatives of the mandibular arch and raise the issue of whether the cleft palate observed in *Moz*−/− pups may be

secondary to defects in lower jaw development, because severe shortening of the mandible, as seen in *Dxl5*−/− foetuses, can affect tongue placement and, secondarily, palate development. However, *Moz*−/− and *Moz*+/−;*Dlx5*+/− mandibles were only slightly shorter (∼10%) and were similar to *Dlx5*+/− mandibles, which do not have palate clefting. Therefore, the only slightly shortened *Moz*−/− mandibles cannot explain the interesting relationship between MOZ activation of the *Dlx5* locus and clefting of the palate. We propose that the combined effect of loss of MOZ on the expression of the entire Dlx gene family and other genes results in cleft palate and other craniofacial anomalies observed in the *Moz*−/− mice. In addition, a number of findings suggest a palate intrinsic effect of MOZ. *Moz* single homozygous mutant animals displayed a delay in palatal shelf elevation and a reduction in horizontal growth, while surrounding structures appeared comparably normal. This was accompanied by a small reduction in BrdU-positive cells in the neural crest-derived mesenchymal cells of palatal shelves of about 15% at a rostrocaudal level, where the palatal shelves first meet in the midline and commence fusion. Although 15% may appear to be a modest reduction in cells in S phase, compounded over only four cell cycles, a 15% reduction in cells in each S phase results in a ∼50% reduction in tissue size $[(1-0.15)^4=0.52]$. These findings suggest that intrinsic defects in mesenchymal cell proliferation contribute to the cleft palate phenotype. In conclusion, we have identified changes in the molecular program underlying craniofacial development that manifest in the absence of the histone acetyltransferase MOZ, providing evidence for a molecular mechanism that potentially causes the craniofacial anomalies seen in individuals with the *KAT6A* (*MOZ*) heterozygous mutation syndrome.

MATERIALS AND METHODS
Mice
All animal experiments (*Mus musculus*) were approved by the Walter and Eliza Hall Institute Animal Ethics Committee and conducted in accordance with the Australian code of practice for the care and use of animals for scientific purposes. For timed matings, midday following the detection of a vaginal plug in the morning was designated embryonic day (E) 0.5. Four previously described *Moz* alleles were used for this study: (1) exon 16 truncated *Moz*Δ mice (no protein detectable, therefore null) on a mixed FVB×BALB/c background (Thomas et al., 2006), and (2) exons 3 to 7 *loxP*-flanked *Moz*lox mice (null allele; Voss et al., 2009), (3) exons 3 to 7 deleted *Moz*− mice (Voss et al., 2009) and (4) *Flag-V5-Bio* 3′-tagged *Moz*V5 mice (Sheikh et al., 2015c; Vanyai et al., 2015) maintained on a C57BL/6 background. Depending on the genetic background, animals homozygous for the *Moz*− allele die between E15.5 and birth with 100% penetrance due to developmental defects that are individually lethal, namely cleft palate, a ventricular septum defect and an interrupted aortic arch (Voss et al., 2012). In contrast, *Moz*V5/V5 mice are viable, healthy and fertile, indicating that the *Moz*V5 allele produces functional protein. C57BL/6 *Moz*−/− were used for mid-gestational molecular work, while *Moz*−/− on a mixed genetic background, as well as FVB×BALB/c *Moz*Δ/Δ animals were used to characterise morphological defects at late gestation. The *Moz*− allele on a mixed genetic background was also used in whole-mount *in situ* hybridisation and RT-qPCR experiments. *Moz*− mice on an inbred C57BL/6 background were used for the genetic interaction experiments with *Dlx5*− mice (Depew et al., 1999), also on the C57BL/6 background. *Moz*lox mice on a C57BL/6 background were used for neural crest-specific deletion using *Wnt1-cre*T/+ transgenic mice (Danielian et al., 1998), also on a C57BL/6 background.

Skeletal and histological preparations
Skeletal preparations were performed as previously described (Thomas et al., 2000). Whole embryo heads were fixed overnight in 4% paraformaldehyde (E13.5-15.5) or for 3 days in Bouin's fixative (E18.5) before serial sectioning and Hematoxylin and Eosin staining according to standard histological protocols.

DEVELOPMENT

Whole-mount *in situ* hybridisation and qPCR

Whole-mount *in situ* hybridisation was conducted using standard protocols (Thomas et al., 2007) using sense and antisense cDNA probes detailed in Table S6. qPCR was performed on ChIP genomic DNA or cDNA following reverse transcription (RT) using Superscript III (Life Technologies) on the LightCycler 480 (Roche) using SYBR-green technology (SensiMix, Bioline). qPCR primers are listed in Table S7.

Isolation of pharyngeal arch cells and FACS cell cycle analysis

Primary murine pharyngeal arch cells were isolated in the following manner. E10.5 first and second pharyngeal arches were dissected from individual embryos, transferred into 25 µl of 0.125% trypsin/EDTA solution and incubated for 10 min on ice, then for 2 min at 37°C. Culture medium [175 µl neural stem cell medium (Merson et al., 2006) with 5% ESC-qualified FBS] was added. The pharyngeal arches were dissociated by gentle pipetting. Cells were centrifuged at 200 *g* and resuspended in culture medium.

For cell cycle analysis by fluorescence-activated flow cytometry, cells were fixed in 500 µl of cytofix/cytoperm solution (BD Pharmingen) for 30 min on ice, washed in Perm/Wash solution (BD Pharmingen) and then incubated for 5 min in Perm/Wash solution. Cells were centrifuged, resuspended in residual buffer and split into two: one aliquot was incubated with 20 µl anti-Ki67 (FITC-conjugated anti-Ki-67, BD Pharmingen, 556026) and the other was incubated with isotype control antibody at 4°C overnight. Cells were washed twice in KDS-BSS +2% FCS buffer and resuspended in 200 µl with a 1 µg/ml final concentration of DAPI in deionised H_2O and incubated at room temperature for 30 min. Cells were washed twice in KDS +2% FCS buffer then sieved into a single cell suspension and analysed using a flow cytometer (LSRIIC Becton, Dickinson and Company).

Assessment of cell proliferation and cell death in palatal shelves

E13.5 pregnant mice were injected with a single dose of 100 mg/kg BrdU intraperitoneally and embryos recovered 1 h later. BrdU-treated E13.5 heads were fixed in 4% paraformaldehyde, embedded in paraffin wax and serially sectioned. Frontal sections of rostral, intermediate and caudal palatal shelves were processed for anti-BrdU immunostaining and detection of genomic DNA fragmentation by TUNEL staining on adjacent sections as described previously (Thomas et al., 2000). BrdU- and TUNEL-positive cells were counted on both sides of the entire cross-section of the palatal shelves at three rostro-caudal levels.

Chromatin immunoprecipitation

ChIP followed by qPCR was essentially performed as previously described (Voss et al., 2012) with the modifications described (Vanyai et al., 2015). Specifically, microdissected pharyngeal arch tissue was prepared and sheared under the conditions described previously (Vanyai et al., 2015). ChIP was performed using antibodies against H3K9ac (Cell Signaling, #9649S) and H3K14ac (Cell Signaling, #7627S) in conjunction with magnetic beads or using agarose bead-bound anti-V5 antibody (Sigma, A7345). Anti-H3K9ac and anti-H3K14ac data are displayed as ChIP signal enrichment over a precipitated internal control region (*B2M*); anti-V5 is displayed relative to input fraction. Gene loci were drawn based on the UCSC Genome Browser (genome.ucsc.edu).

ChIP-seq analysis

Single-end ChIP sequencing reads were aligned to the mouse mm10 genome using Rsubread (Liao et al., 2013), and BAM files were generated and processed using SeqMonk Mapped Sequence Data Analyser Version 0.29.0 (Brabraham Institute, Cambridge, UK). Peaks were identified using MACS peak caller.

RNA isolation

For RNA-sequencing and RT-qPCR, total RNA was isolated from the maxillary component of the 1st pharyngeal arch at E10.5 and E11.5, from the palatal shelves at E13.5 and E14.0, and from E10.5 1st and 2nd pharyngeal arches (RNAeasy, Qiagen) from embryos on a C57BL/6 background.

RNA sequencing

Uniquely indexed libraries were generated per sample with the TruSeq Stranded mRNA LT Sample Prep Kit (Illumina), according to manufacturer's instructions. Indexed libraries were sequenced on the NextSeq platform (Illumina), generating 75 bp single end reads, yielding a minimum of ~15 million total reads per sample.

RNA-seq analysis

Sequence reads were aligned to the mouse mm10 genome using Rsubread (Liao et al., 2013). Mapped reads were assigned to Entrez genes using featureCounts (Liao et al., 2014) and the in-built RefSeq annotation in Rsubread. Gene annotation was downloaded from the NCBI (ftp:// ftp.ncbi.nlm.nih.gov). Differential expression analyses were undertaken using the edgeR (Robinson et al., 2010) and limma (Ritchie et al., 2015) software packages. Genes were filtered from the analysis if they failed to achieve at least 0.5 counts per million reads (CPM) in at least four samples. Genes without current annotation were also removed. Libraries were scale normalised using the trimmed mean of log expression ratios (TMM) method (Robinson and Oshlack, 2010). Counts were transformed to $\log_2$ counts per million with associated precision weights using voom (Law et al., 2014). Differential expression was assessed using linear models and robust empirical Bayes moderated t-statistics (Phipson et al., 2016). *P* values were adjusted to control the false discovery rate (FDR) below 5% using the Benjamini and Hochberg method. To increase precision, the linear models incorporated corrections for a batch effect and two surrogate variables. The batch effect adjusted for two mouse colony locations. The surrogate variables were computed from a singular value decomposition of the linear model residuals. Expression signature analysis of the differential expression results was conducted using rotation gene set tests (ROAST; Wu et al., 2010). Gene ontology analyses were conducted using limma's goana function.

To make multidimensional scaling plots (MDS) and heatmaps, the expression of each gene was summarised as a $\log_2$-CPM value using the cpm function of edgeR, with a prior count of 5, and batch effects were removed using the removeBatchEffects function in limma. The plots themselves were made using the plotMDS and heatmap.2 functions. Distances on the MDS plot represent leading $\log_2$ fold-change, which is the root-mean-square average of the largest 500 $\log_2$ fold-changes between each pair of RNA samples. Heatmap *z*-values were standardized to have mean 0 and standard deviation 1 for each gene, and hierarchical clustering was applied to the genes. RNA-seq read distribution over the exons of the *Moz* locus are displayed in Fig. S1 and show loss of reads over the deleted exons 3 to 7 in the $Moz^{-/-}$ E10.5 pharyngeal arches.

Statistical analysis

The number of observations used was calculated to enable detection of a 25% difference between genotypes at alpha 0.05 with 80% power. Embryos and pups were examined blinded to genotype, i.e. before genotyping, and machine data generation was used to avoid bias where possible (RNA-seq, ChIP-seq, RT-qPCR, FACS). No animals were excluded. The number of observations and the statistical tests used are specified in the figure legends.

Competing interests

The authors declare no competing or financial interests.

Author contributions

Conceptualization: H.K.V., G.K.S., T.T., A.K.V.; Methodology: H.K.V., R.E.M., H.M.M., C.C., S.W., T.T.; Software: G.K.S.; Validation: H.K.V., R.E.M., G.K.S.; Formal analysis: H.K.V., A.G., A.K.V.; Investigation: H.K.V., R.E.M., H.M.M., C.C., S.W., T.T.; Data curation: A.G., A.K.V.; Writing - original draft: H.K.V., G.K.S., A.K.V.; Writing - review & editing: T.T., A.K.V.; Visualization: H.K.V., A.K.V.; Supervision: G.K.S., T.T., A.K.V.; Project administration: T.T., A.K.V.; Funding acquisition: T.T., A.K.V.

DEVELOPMENT

Data availability

ChIP-seq and RNA-seq data have been deposited in GEO and are listed under the super-series accession number GSE134609. The ChIP-seq data accession number is GSE134607 and the RNA-seq data accession number is GSE134608.

Supplementary information

Supplementary information available online at
http://dev.biologists.org/lookup/doi/10.1242/dev.175042.supplemental

References

Acampora, D., Merlo, G. R., Paleari, L., Zerega, B., Postiglione, M. P., Mantero, S., Bober, E., Barbieri, O., Simeone, A. and Levi, G. (1999). Craniofacial, vestibular and bone defects in mice lacking the Distal-less-related gene Dlx5. *Development* 126, 3795-3809.

Arboleda, V. A., Lee, H., Dorrani, N., Zadeh, N., Willis, M., Macmurdo, C. F., Manning, M. A., Kwan, A., Hudgins, L., Barthelemy, F. et al. (2015). De novo nonsense mutations in KAT6A, a lysine acetyl-transferase gene, cause a syndrome including microcephaly and global developmental delay. *Am. J. Hum. Genet.* 96, 498-506. doi:10.1016/j.ajhg.2015.01.017

Barron, F., Woods, C., Kuhn, K., Bishop, J., Howard, M. J. and Clouthier, D. E. (2011). Downregulation of Dlx5 and Dlx6 expression by Hand2 is essential for initiation of tongue morphogenesis. *Development* 138, 2249-2259. doi:10.1242/dev.056929

Bhatt, S., Diaz, R. and Trainor, P. A. (2013). Signals and switches in Mammalian neural crest cell differentiation. *Cold Spring Harb. Perspect. Biol.* 5, a008326. doi:10.1101/cshperspect.a008326

Borrow, J., Stanton, V. P., Jr., Andresen, J. M., Becher, R., Behm, F. G., Chaganti, R. S. K., Civin, C. I., Disteche, C., Dubé, I., Frischauf, A. M. et al. (1996). The translocation t(8;16)(p11;p13) of acute myeloid leukaemia fuses a putative acetyltransferase to the CREB-binding protein. *Nat. Genet.* 14, 33-41. doi:10.1038/ng0996-33

Bush, J. O. and Jiang, R. (2012). Palatogenesis: morphogenetic and molecular mechanisms of secondary palate development. *Development* 139, 231-243. doi:10.1242/dev.067082

Campeau, P. M., Kim, J. C., Lu, J. T., Schwartzentruber, J. A., Abdul-Rahman, O. A., Schlaubitz, S., Murdock, D. M., Jiang, M.-M., Lammer, E. J., Enns, G. M. et al. (2012). Mutations in KAT6B, encoding a histone acetyltransferase, cause Genitopatellar syndrome. *Am. J. Hum. Genet.* 90, 282-289. doi:10.1016/j.ajhg.2011.11.023

Charite, J., McFadden, D. G., Merlo, G., Levi, G., Clouthier, D. E., Yanagisawa, M., Richardson, J. A. and Olson, E. N. (2001). Role of Dlx6 in regulation of an endothelin-1-dependent, dHAND branchial arch enhancer. *Genes Dev.* 15, 3039-3049. doi:10.1101/gad.931701

Clayton-Smith, J., O'Sullivan, J., Daly, S., Bhaskar, S., Day, R., Anderson, B., Voss, A. K., Thomas, T., Biesecker, L. G., Smith, P. et al. (2011). Whole-exome-sequencing identifies mutations in histone acetyltransferase gene KAT6B in individuals with the Say-Barber-Biesecker variant of Ohdo syndrome. *Am. J. Hum. Genet.* 89, 675-681. doi:10.1016/j.ajhg.2011.10.008

Crump, J. G., Swartz, M. E., Eberhart, J. K. and Kimmel, C. B. (2006). Moz-dependent Hox expression controls segment-specific fate maps of skeletal precursors in the face. *Development* 133, 2661-2669. doi:10.1242/dev.02435

Danielian, P. S., Muccino, D., Rowitch, D. H., Michael, S. K. and McMahon, A. P. (1998). Modification of gene activity in mouse embryos in utero by a tamoxifen-inducible form of Cre recombinase. *Curr. Biol.* 8, 1323-1326. doi:10.1016/S0960-9822(07)00562-3

Depew, M. J., Liu, J. K., Long, J. E., Presley, R., Meneses, J. J., Pedersen, R. A. and Rubenstein, J. L. (1999). Dlx5 regulates regional development of the branchial arches and sensory capsules. *Development* 126, 3831-3846.

Depew, M. J., Lufkin, T. and Rubenstein, J. L. (2002). Specification of jaw subdivisions by Dlx genes. *Science* 298, 381-385. doi:10.1126/science.1075703

Depew, M. J., Simpson, C. A., Morasso, M. and Rubenstein, J. L. R. (2005). Reassessing the Dlx code: the genetic regulation of branchial arch skeletal pattern and development. *J. Anat.* 207, 501-561. doi:10.1111/j.1469-7580.2005.00487.x

Diez-Roux, G., Banfi, S., Sultan, M., Geffers, L., Anand, S., Rozado, D., Magen, A., Canidio, E., Pagani, M., Peluso, I. et al. (2011). A high-resolution anatomical atlas of the transcriptome in the mouse embryo. *PLoS Biol.* 9, e1000582. doi:10.1371/journal.pbio.1000582

Dixon, M. J., Marazita, M. L., Beaty, T. H. and Murray, J. C. (2011). Cleft lip and palate: understanding genetic and environmental influences. *Nat. Rev. Genet.* 12, 167-178. doi:10.1038/nrg2933

Ducy, P., Zhang, R., Geoffroy, V., Ridall, A. L. and Karsenty, G. (1997). Osf2/Cbfa1: a transcriptional activator of osteoblast differentiation. *Cell* 89, 747-754. doi:10.1016/S0092-8674(00)80257-3

Elliott, A. M. and Evans, J. A. (2006). Genotype-phenotype correlations in mapped split hand foot malformation (SHFM) patients. *Am. J. Med. Genet. A* 140A, 1419-1427. doi:10.1002/ajmg.a.31244

Engleka, K. A., Wu, M., Zhang, M., Antonucci, N. B. and Epstein, J. A. (2007). Menin is required in cranial neural crest for palatogenesis and perinatal viability. *Dev. Biol.* 311, 524-537. doi:10.1016/j.ydbio.2007.08.057

Fortschegger, K., de Graaf, P., Outchkourov, N. S., van Schaik, F. M. A., Timmers, H. T. M. and Shiekhattar, R. (2010). PHF8 targets histone methylation and RNA polymerase II to activate transcription. *Mol. Cell. Biol.* 30, 3286-3298. doi:10.1128/MCB.01520-09

Garofalo, S., Vuorio, E., Metsaranta, M., Rosati, R., Toman, D., Vaughan, J., Lozano, G., Mayne, R., Ellard, J., Horton, W. et al. (1991). Reduced amounts of cartilage collagen fibrils and growth plate anomalies in transgenic mice harboring a glycine-to-cysteine mutation in the mouse type II procollagen alpha 1-chain gene. *Proc. Natl. Acad. Sci. USA* 88, 9648-9652. doi:10.1073/pnas.88.21.9648

Good-Jacobson, K. L., Chen, Y., Voss, A. K., Smyth, G. K., Thomas, T. and Tarlinton, D. (2014). Regulation of germinal center responses and B-cell memory by the chromatin modifier MOZ. *Proc. Natl. Acad. Sci. USA* 111, 9585-9590. doi:10.1073/pnas.1402485111

Grabow, S., Kueh, A. J., Ke, F., Vanyai, H. K., Sheikh, B. N., Dengler, M. A., Chiang, W., Eccles, S., Smyth, I. M., Jones, L. K. et al. (2018). Subtle changes in the levels of BCL-2 proteins cause severe craniofacial abnormalities. *Cell Rep.* 24, 3285-3295.e3284. doi:10.1016/j.celrep.2018.08.048

Green, P. D., Hjalt, T. A., Kirk, D. E., Sutherland, L. B., Thomas, B. L., Sharpe, P. T., Snead, M. L., Murray, J. C., Russo, A. F. and Amendt, B. A. (2001). Antagonistic regulation of Dlx2 expression by PITX2 and Msx2: implications for tooth development. *Gene Expr.* 9, 265-281. doi:10.3727/000000001783992515

Gritli-Linde, A. (2007). Molecular control of secondary palate development. *Dev. Biol.* 301, 309-326. doi:10.1016/j.ydbio.2006.07.042

Gritli-Linde, A. (2008). The etiopathogenesis of cleft lip and cleft palate: usefulness and caveats of mouse models. *Curr. Top. Dev. Biol.* 84, 37-138. doi:10.1016/S0070-2153(08)00602-9

Grosen, D., Bille, C., Petersen, I., Skytthe, A., Hjelmborg, J. B., Pedersen, J. K., Murray, J. C. and Christensen, K. (2011). Risk of oral clefts in twins. *Epidemiology* 22, 313-319. doi:10.1097/EDE.0b013e3182125f9c

Han, J., Mayo, J., Xu, X., Li, J., Bringas, P., Jr., Maas, R. L., Rubenstein, J. L. R. and Chai, Y. (2009). Indirect modulation of Shh signaling by Dlx5 affects the oral-nasal patterning of palate and rescues cleft palate in Msx1-null mice. *Development* 136, 4225-4233. doi:10.1242/dev.036723

Hartmann, C. (2009). Transcriptional networks controlling skeletal development. *Curr. Opin. Genet. Dev.* 19, 437-443. doi:10.1016/j.gde.2009.09.001

Herbrand, H., Pabst, O., Hill, R. and Arnold, H.-H. (2002). Transcription factors Nkx3.1 and Nkx3.2 (Bapx1) play an overlapping role in sclerotomal development of the mouse. *Mech. Dev.* 117, 217-224. doi:10.1016/S0925-4773(02)00207-1

Hojo, H., Ohba, S., He, X., Lai, L. P. and McMahon, A. P. (2016). Sp7/Osterix is restricted to bone-forming vertebrates where it acts as a Dlx co-factor in osteoblast specification. *Dev. Cell* 37, 238-253. doi:10.1016/j.devcel.2016.04.002

Horike, S.-I., Cai, S., Miyano, M., Cheng, J.-F. and Kohwi-Shigematsu, T. (2005). Loss of silent-chromatin looping and impaired imprinting of DLX5 in Rett syndrome. *Nat. Genet.* 37, 31-40. doi:10.1038/ng1491

Jeong, J., Li, X., McEvilly, R. J., Rosenfeld, M. G., Lufkin, T. and Rubenstein, J. L. R. (2008). Dlx genes pattern mammalian jaw primordium by regulating both lower jaw-specific and upper jaw-specific genetic programs. *Development* 135, 2905-2916. doi:10.1242/dev.019778

Jeong, J., Cesario, J., Zhao, Y., Burns, L., Westphal, H. and Rubenstein, J. L. R. (2012). Cleft palate defect of Dlx1/2–/– mutant mice is caused by lack of vertical outgrowth in the posterior palate. *Dev. Dyn.* 241, 1757-1769. doi:10.1002/dvdy.23867

Jiang, Z., Pan, L., Chen, X., Chen, Z. and Xu, D. (2017). Wnt6 influences the viability of mouse embryonic palatal mesenchymal cells via the beta-catenin pathway. *Exp. Ther. Med.* 14, 5339-5344. doi:10.3892/etm.2017.5240

Katsumoto, T., Aikawa, Y., Iwama, A., Ueda, S., Ichikawa, H., Ochiya, T. and Kitabayashi, I. (2006). MOZ is essential for maintenance of hematopoietic stem cells. *Genes Dev.* 20, 1321-1330. doi:10.1101/gad.1393106

Ke, F. F. S., Vanyai, H. K., Cowan, A. D., Delbridge, A. R. D., Whitehead, L., Grabow, S., Czabotar, P. E., Voss, A. K. and Strasser, A. (2018). Embryogenesis and Adult Life in the Absence of Intrinsic Apoptosis Effectors BAX, BAK, and BOK. *Cell* 173, 1217-1230.e1217. doi:10.1016/j.cell.2018.04.036

Kern, B., Shen, J., Starbuck, M. and Karsenty, G. (2001). Cbfa1 contributes to the osteoblast-specific expression of type I collagen genes. *J. Biol. Chem.* 276, 7101-7107. doi:10.1074/jbc.M006215200

Komori, T., Yagi, H., Nomura, S., Yamaguchi, A., Sasaki, K., Deguchi, K., Shimizu, Y., Bronson, R. T., Gao, Y.-H., Inada, M. et al. (1997). Targeted disruption of Cbfa1 results in a complete lack of bone formation owing to maturational arrest of osteoblasts. *Cell* 89, 755-764. doi:10.1016/S0092-8674(00)80258-5

Lan, Y., Xu, J. and Jiang, R. (2015). Cellular and molecular mechanisms of palatogenesis. *Curr. Top. Dev. Biol.* 115, 59-84. doi:10.1016/bs.ctdb.2015.07.002

Laumonnier, F., Holbert, S., Ronce, N., Faravelli, F., Lenzner, S., Schwartz, C. E., Lespinasse, J., Van Esch, H., Lacombe, D., Goizet, C. et al. (2005). Mutations in PHF8 are associated with X linked mental retardation and cleft lip/cleft palate. J. Med. Genet. 42, 780-786. doi:10.1136/jmg.2004.029439

Law, C. W., Chen, Y., Shi, W. and Smyth, G. K. (2014). voom: precision weights unlock linear model analysis tools for RNA-seq read counts. Genome Biol. 15, R29. doi:10.1186/gb-2014-15-2-r29

Lefebvre, V. and Bhattaram, P. (2010). Vertebrate skeletogenesis. Curr. Top. Dev. Biol. 90, 291-317. doi:10.1016/S0070-2153(10)90008-2

Lefebvre, V., Huang, W., Harley, V. R., Goodfellow, P. N. and de Crombrugghe, B. (1997). SOX9 is a potent activator of the chondrocyte-specific enhancer of the pro alpha1(II) collagen gene. Mol. Cell. Biol. 17, 2336-2346. doi:10.1128/MCB.17.4.2336

Liao, Y., Smyth, G. K. and Shi, W. (2013). The Subread aligner: fast, accurate and scalable read mapping by seed-and-vote. Nucleic Acids Res. 41, e108. doi:10.1093/nar/gkt214

Liao, Y., Smyth, G. K. and Shi, W. (2014). featureCounts: an efficient general purpose program for assigning sequence reads to genomic features. Bioinformatics 30, 923-930. doi:10.1093/bioinformatics/btt656

Lindgren, A. M., Hoyos, T., Talkowski, M. E., Hanscom, C., Blumenthal, I., Chiang, C., Ernst, C., Pereira, S., Ordulu, Z., Clericuzio, C. et al. (2013). Haploinsufficiency of KDM6A is associated with severe psychomotor retardation, global growth restriction, seizures and cleft palate. Hum. Genet. 132, 537-552. doi:10.1007/s00439-013-1263-x

Loenarz, C., Ge, W., Coleman, M. L., Rose, N. R., Cooper, C. D. O., Klose, R. J., Ratcliffe, P. J. and Schofield, C. J. (2010). PHF8, a gene associated with cleft lip/palate and mental retardation, encodes for an Nε-dimethyl lysine demethylase. Hum. Mol. Genet. 19, 217-222. doi:10.1093/hmg/ddp480

Merson, T. D., Dixon, M. P., Collin, C., Rietze, R. L., Bartlett, P. F., Thomas, T. and Voss, A. K. (2006). The transcriptional coactivator Querkopf controls adult neurogenesis. J. Neurosci. 26, 11359-11370. doi:10.1523/JNEUROSCI.2247-06.2006

Millan, F., Cho, M. T., Retterer, K., Monaghan, K. G., Bai, R., Vitazka, P., Everman, D. B., Smith, B., Angle, B., Roberts, V. et al. (2016). Whole exome sequencing reveals de novo pathogenic variants in KAT6A as a cause of a neurodevelopmental disorder. Am. J. Med. Genet. A 170, 1791-1798. doi:10.1002/ajmg.a.37670

Miller, C. T., Maves, L. and Kimmel, C. B. (2004). moz regulates Hox expression and pharyngeal segmental identity in zebrafish. Development 131, 2443-2461. doi:10.1242/dev.01134

Newman, D. M., Sakaguchi, S., Lun, A., Preston, S., Pellegrini, M., Khamina, K., Bergthaler, A., Nutt, S. L., Smyth, G. K., Voss, A. K. et al. (2016). Acetylation of the Cd8 locus by KAT6A determines memory T cell diversity. Cell Rep. 16, 3311-3321. doi:10.1016/j.celrep.2016.08.056

Otto, F., Thornell, A. P., Crompton, T., Denzel, A., Gilmour, K. C., Rosewell, I. R., Stamp, G. W. H., Beddington, R. S. P., Mundlos, S., Olsen, B. R. et al. (1997). Cbfa1, a candidate gene for cleidocranial dysplasia syndrome, is essential for osteoblast differentiation and bone development. Cell 89, 765-771. doi:10.1016/S0092-8674(00)80259-7

Peters, H., Neubuser, A., Kratochwil, K. and Balling, R. (1998). Pax9-deficient mice lack pharyngeal pouch derivatives and teeth and exhibit craniofacial and limb abnormalities. Genes Dev. 12, 2735-2747. doi:10.1101/gad.12.17.2735

Phipson, B., Lee, S., Majewski, I. J., Alexander, W. S. and Smyth, G. K. (2016). Robust hyperparameter estimation protects against hypervariable genes and improves power to detect differential expression. Ann. Appl. Stat. 10, 946-963. doi:10.1214/16-AOAS920

Qiu, M., Bulfone, A., Martinez, S., Meneses, J. J., Shimamura, K., Pedersen, R. A. and Rubenstein, J. L. (1995). Null mutation of Dlx-2 results in abnormal morphogenesis of proximal first and second branchial arch derivatives and abnormal differentiation in the forebrain. Genes Dev. 9, 2523-2538. doi:10.1101/gad.9.20.2523

Qiu, M., Bulfone, A., Ghattas, I., Meneses, J. J., Christensen, L., Sharpe, P. T., Presley, R., Pedersen, R. A. and Rubenstein, J. L. R. (1997). Role of the Dlx homeobox genes in proximodistal patterning of the branchial arches: mutations of Dlx-1, Dlx-2, and Dlx-1 and −2 alter morphogenesis of proximal skeletal and soft tissue structures derived from the first and second arches. Dev. Biol. 185, 165-184. doi:10.1006/dbio.1997.8556

Reymond, A., Marigo, V., Yaylaoglu, M. B., Leoni, A., Ucla, C., Scamuffa, N., Caccioppoli, C., Dermitzakis, E. T., Lyle, R., Banfi, S. et al. (2002). Human chromosome 21 gene expression atlas in the mouse. Nature 420, 582-586. doi:10.1038/nature01178

Ritchie, M. E., Phipson, B., Wu, D., Hu, Y., Law, C. W., Shi, W. and Smyth, G. K. (2015). limma powers differential expression analyses for RNA-sequencing and microarray studies. Nucleic Acids Res. 43, e47. doi:10.1093/nar/gkv007

Robinson, M. D. and Oshlack, A. (2010). A scaling normalization method for differential expression analysis of RNA-seq data. Genome Biol. 11, R25. doi:10.1186/gb-2010-11-3-r25

Robinson, M. D., McCarthy, D. J. and Smyth, G. K. (2010). edgeR: a Bioconductor package for differential expression analysis of digital gene expression data. Bioinformatics 26, 139-140. doi:10.1093/bioinformatics/btp616

Sheikh, B. N., Downer, N. L., Phipson, B., Vanyai, H. K., Kueh, A. J., McCarthy, D. J., Smyth, G. K., Thomas, T. and Voss, A. K. (2015a). MOZ and BMI1 play opposing roles during Hox gene activation in ES cells and in body segment identity specification in vivo. Proc. Natl. Acad. Sci. USA 112, 5437-5442. doi:10.1073/pnas.1422872112

Sheikh, B. N., Lee, S. C. W., El-Saafin, F., Vanyai, H. K., Hu, Y., Pang, S. H. M., Grabow, S., Strasser, A., Nutt, S. L., Alexander, W. S. et al. (2015b). MOZ regulates B-cell progenitors and, consequently, Moz haploinsufficiency dramatically retards MYC-induced lymphoma development. Blood 125, 1910-1921. doi:10.1182/blood-2014-08-594655

Sheikh, B. N., Phipson, B., El-Saafin, F., Vanyai, H. K., Downer, N. L., Bird, M. J., Kueh, A. J., May, R. E., Smyth, G. K., Voss, A. K. et al. (2015c). MOZ (MYST3, KAT6A) inhibits senescence via the INK4A-ARF pathway. Oncogene 34, 5807-5820. doi:10.1038/onc.2015.33

Sheikh, B. N., Yang, Y., Schreuder, J., Nilsson, S. K., Bilardi, R., Carotta, S., McRae, H. M., Metcalf, D., Voss, A. K. and Thomas, T. (2016). MOZ (KAT6A) is essential for the maintenance of classically defined adult hematopoietic stem cells. Blood blood-2015-10-676072. doi:10.1182/blood-2015-10-676072

Shoulders, M. D. and Raines, R. T. (2009). Collagen structure and stability. Annu. Rev. Biochem. 78, 929-958. doi:10.1146/annurev.biochem.77.032207.120833

Snead, M. P. and Yates, J. R. (1999). Clinical and Molecular genetics of Stickler syndrome. J. Med. Genet. 36, 353-359.

Sperry, E. D., Hurd, E. A., Durham, M. A., Reamer, E. N., Stein, A. B. and Martin, D. M. (2014). The chromatin remodeling protein CHD7, mutated in CHARGE syndrome, is necessary for proper craniofacial and tracheal development. Dev. Dyn. 243, 1055-1066. doi:10.1002/dvdy.24156

Stricker, S., Fundele, R., Vortkamp, A. and Mundlos, S. (2002). Role of Runx genes in chondrocyte differentiation. Dev. Biol. 245, 95-108. doi:10.1006/dbio.2002.0640

Takarada, T., Nakazato, R., Tsuchikane, A., Fujikawa, K., Iezaki, T., Yoneda, Y. and Hinoi, E. (2016). Genetic analysis of Runx2 function during intramembranous ossification. Development 143, 211-218. doi:10.1242/dev.128793

Tham, E., Lindstrand, A., Santani, A., Malmgren, H., Nesbitt, A., Dubbs, H. A., Zackai, E. H., Parker, M. J., Millan, F., Rosenbaum, K. et al. (2015). Dominant mutations in KAT6A cause intellectual disability with recognizable syndromic features. Am. J. Hum. Genet. 96, 507-513. doi:10.1016/j.ajhg.2015.01.016

Thomas, T., Voss, A. K., Chowdhury, K. and Gruss, P. (2000). Querkopf, a MYST family histone acetyltransferase, is required for normal cerebral cortex development. Development 127, 2537-2548.

Thomas, T., Corcoran, L. M., Gugasyan, R., Dixon, M. P., Brodnicki, T., Nutt, S. L., Metcalf, D. and Voss, A. K. (2006). Monocytic leukemia zinc finger protein is essential for the development of long-term reconstituting hematopoietic stem cells. Genes Dev. 20, 1175-1186. doi:10.1101/gad.1382606

Thomas, T., Loveland, K. L. and Voss, A. K. (2007). The genes coding for the MYST family histone acetyltransferases, Tip60 and Mof, are expressed at high levels during sperm development. Gene Expr. Patterns 7, 657-665. doi:10.1016/j.modgep.2007.03.005

Tunovic, S., Barkovich, J., Sherr, E. H. and Slavotinek, A. M. (2014). De novo ANKRD11 and KDM1A gene mutations in a male with features of KBG syndrome and Kabuki syndrome. Am. J. Med. Genet. A 164, 1744-1749. doi:10.1002/ajmg.a.36450

Vanyai, H. K., Thomas, T. and Voss, A. K. (2015). Mesodermal expression of Moz is necessary for cardiac septum development. Dev. Biol. 403, 22-29. doi:10.1016/j.ydbio.2015.04.011

Venugopalan, S. R., Li, X., Amen, M. A., Florez, S., Gutierrez, D., Cao, H., Wang, J. and Amendt, B. A. (2011). Hierarchical interactions of homeodomain and forkhead transcription factors in regulating odontogenic gene expression. J. Biol. Chem. 286, 21372-21383. doi:10.1074/jbc.M111.252031

Verzi, M. P., Agarwal, P., Brown, C., McCulley, D. J., Schwarz, J. J. and Black, B. L. (2007). The transcription factor MEF2C is required for craniofacial development. Dev. Cell 12, 645-652. doi:10.1016/j.devcel.2007.03.007

Voss, A. K., Collin, C., Dixon, M. P. and Thomas, T. (2009). Moz and retinoic acid coordinately regulate H3K9 acetylation, Hox gene expression, and segment identity. Dev. Cell 17, 674-686. doi:10.1016/j.devcel.2009.10.006

Voss, A. K., Vanyai, H. K., Collin, C., Dixon, M. P., McLennan, T. J., Sheikh, B. N., Scambler, P. and Thomas, T. (2012). MOZ regulates the Tbx1 locus, and Moz mutation partially phenocopies DiGeorge syndrome. Dev. Cell 23, 652-663. doi:10.1016/j.devcel.2012.07.010

Walker, B. E. and Fraser, F. C. (1956). Closure of the secondary palate in three strains of mice. J. Embryol. Exp. Morphol. 4, 176-189.

Wu, D., Lim, E., Vaillant, F., Asselin-Labat, M.-L., Visvader, J. E. and Smyth, G. K. (2010). ROAST: rotation gene set tests for complex microarray experiments. Bioinformatics 26, 2176-2182. doi:10.1093/bioinformatics/btq401

Wu, D., Mandal, S., Choi, A., Anderson, A., Prochazkova, M., Perry, H., Gil-Da-Silva-Lopes, V. L., Lao, R., Wan, E., Tang, P. L.-F. et al. (2015). DLX4 is associated with orofacial clefting and abnormal jaw development. Hum. Mol. Genet. 24, 4340-4352. doi:10.1093/hmg/ddv167

Yu, K. and Ornitz, D. M. (2011). Histomorphological study of palatal shelf elevation during murine secondary palate formation. Dev. Dyn. 240, 1737-1744. doi:10.1002/dvdy.22670

Zhou, G., Zheng, Q., Engin, F., Munivez, E., Chen, Y., Sebald, E., Krakow, D. and Lee, B. (2006). Dominance of SOX9 function over RUNX2 during skeletogenesis. Proc. Natl. Acad. Sci. USA 103, 19004-19009. doi:10.1073/pnas.0605170103

DEVELOPMENT